BIOELECTRIC EFFECTS OF LOW-FREQUENCY MODULATED MICROWAVE FIELDS ON NERVOUS SYSTEM CELLS

María J. Azanza, A. del Moral and R. N. Pérez-Bruzón
University of Zaragoza
Spain

1. Introduction. Cell biology fundamentals of the bioelectric behaviour of neuron plasma membrane underlining the biophysics of the neuron bioelectric impulse.

1.1 Introduction.

In this chapter we present a comprehensive study of the action of applied magnetic fields (MF) (static, alternating of extremely low frequency (ELF) (0.1-217 Hz) and ELF MF modulating microwave (MW) carriers of 9.6 (100 and 800 Hz) and 13.6 GHz (2-100 Hz)). The target is the neuron membrane, and the underlying mechanism explaining the MF effect is the Ca^{2+} ion liberation from its membrane cytosolic stores. The chapter is organized as follows. After studying the bioelectric action potential across membrane, enlarging Hodgkin-Huxley master equations with the Ca^{2+} diffusion current and solving them considering the membrane as a Kirchoff knot, we describe the experimental set-ups. Next we describe and discuss the main effects discovered: bioelectric frequency inhibition and excitation, neuron synchronization under ELF MF, frequency resonance effect ("frequency window" effect), ELF modulated MW demodulation explanation, and also the effect of such a MW on human astrocytoma cells proliferation. A general model based on membrane phospholipids superdiamagnetism (SD) and Ca^{2+} liberation under Coulomb explosion (CE) is described and successfully corroborated by our experimental results. In particular our SD+CE model explains well the so called *frequency window effect*, where only a narrow band-width is effective in the AC MF interaction with the biological systems.

1.2 Molecular structure of plasma membrane.

Neurons cell biology and molecular foundations of bioelectric and synaptic-mediated processes are well defined in terms of: membrane surface structure and membrane molecular components.

According to the lipid globular-protein fluid mosaic model (Singer and Nicolson, 1972) cell membranes main components -lipids and proteins- are organized in a phospholipid (PP) bilayer, being proteins either embedded in one or two of the hemilayers, or located entirely exposed at the external or internal cell surfaces, being attached to the bilayer by a covalent

linkage. The PP bilayer is asymmetric, due in part to the electrical charge lipid molecule distribution, i.e. negatively charged phosphatidylserine (PS) and glycolipids (GL) that are almost exclusively located in the inner and outer halves of the membrane respectively (Rothman and Lenard, 1977) (Fig.1). PS molecules, with their additional functional groups and net negative charge –e in the polar head, interact with cytosolic Ca^{2+} (Papahadjopoulos and Bangham, 1966). Precise information about the exact content of PS in neuron membrane

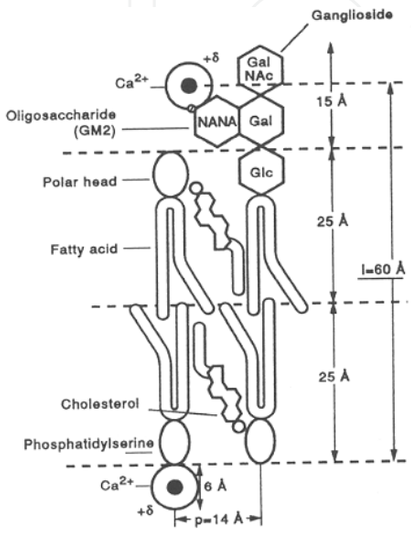

Fig. 1. Model of neuron membrane, showing the PS and a NANA glycolipid with the ganglioside head GM2, both heads negatively charged with –e (modified from Alberts et al., 1989). Bound to the heads are water solvated Ca^{2+}, the overall heads having an effective positive charge +δ. Interposed between the lipids are cholesterol molecules. Also shown are the PP long molecules. The crucial lengths intervening in the model of MF interaction with plasma membrane (see § 3), $l \cong 60$ Å and $p \cong 14$ Å, are shown (del Moral and Azanza, 1992).

is scarce but it is known that they amount ≅ 14% of the half cytosolic lipid bilayer molecules (Alberts et al., 1989). Gangliosides, defined as sialic acid-containing glycosphingolipids, account for an estimated 5-10% of the total lipids in the neuronal plasma membrane, or about 10-20 % in the external half of the bilayer, where they are located. GL can carry one or more –e charges (polyanionic heads) depending upon the number of N-acetylneuraminic acid (sialic acid, NANA) residues, which represent in turn binding sites for Ca^{2+}. Interposed between the lipids are cholesterol molecules with dielectric constant $\varepsilon_r = 2.21$.

1.3 Neuron bioelectric impulse biophysics.

Neurons plasma membranes are organized to generate and propagate *bioelectric* signals, i.e. waves of voltage, the *nerve impulses*, in response to a stimulus. In a resting neuron, at both sides of the plasma membrane, there exits an electric potential difference, *resting potential*, being the inner membrane surface (i) negatively charged (≅ - 60 mV) with respect to the external one (o). Transmembrane potential is produced by a different concentration of ions at both sides of the membrane, as given by well known Nernst equation, $E = (RT/zF)\ln(c_o/c_i)$, where c_i and c_0 are the relevant ion concentrations.

Considering transmembrane diffusible ions e.m.f., there exists in the cytosol a high concentration of K^+ ions while in the extracellular fluid there are higher concentrations (R is the gas constant, F, de Faraday and z, the ion valence) of Na^+, Ca^{2+} and Mg^{2+} ions, being Cl^- ions concentrations variable depending on the kind of neuron. As a stimulus is applied to the membrane, a stimulation threshold arising, arising a stimulation threshold, transmembrane voltage is reversed becoming the inner surface positive, *depolarization*. In few tens of ms the original inner negative potential is recovered (Fig.2). Such a voltage modifications have the shape of an impulse were we can distinguish three main phases: depolarization (D), repolarization (R) and hyperpolarization (H), each one conveyed by a kind of ion. Membrane stimulation induces the opening of either Na^+- or Ca^{2+}-channels. Ions diffuse inside de membrane raising their equilibrium potential according to Nernst equation. As the membrane is depolarizing K^+-channels are opened, allowing the reversion of transmembrane potential. The sorting of K^+ ions charges the membrane negatively, *repolarization*, getting the negative value for K^+ equilibrium potential, *hyperpolarization*. Finally the $3Na^+/2K^+$-exchange pump, plus sorting of Cl^- ions, recovers the initial resting transmembrane potential. Through the non-polar (dielectric) lipid bilayer, ions diffuse across protein-channels. Three kinds of ionic channels are operating in membranes, leakage channels (L), voltage- and ligand-activated channels.

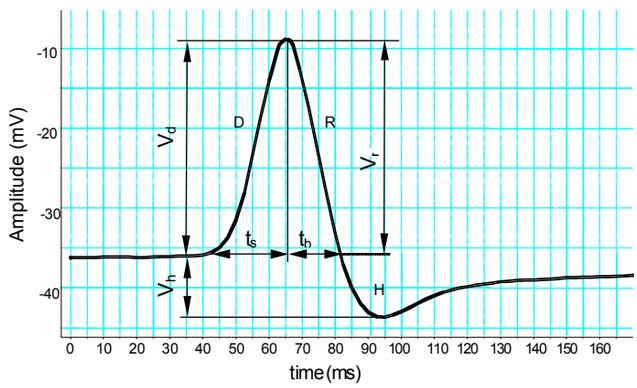

Fig. 2. D: depolarization; R: repolarization; H: hyperpolarization. V_d depolarization voltage; V_h hiperpolarization voltage; V_r repolarization voltage; t_s stimulation time; t_h hyperpolarization time. (Pérez-Bruzón, 2006).

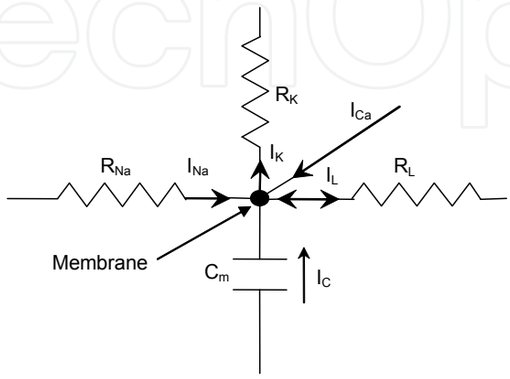

Fig. 3. Plasma membrane as a knot, where ionic currents concur.

The D and H main trams of bioelectric impulse in neurons (Fig. 2) are controlled by the well known Hodgkin & Huxley (HH) equation (Hodgkin and Huxley, 1952). This equation has been usually referred to an equivalent electric circuit of in parallel conductances, membrane capacitance, C_m and DC generators, the latter being mainly the Nernst equilibrium Na^+ and K^+ e.m.f., E_{Na} and E_K, due to the ions electrochemical gradients (other e.m.f. are due to Ca^{2+} and Cl^- ions). Consideration of this network by meshes does not allow its easy solution, and we will consider the membrane as a Kirchoff knot where the currents concur (Fig. 3). Therefore HH equation in the presence of an applied magnetic field, B_{eff}, takes the knot law of charge conservation (no charge accumulation in membrane),

$$C_m(dV/dt)+g_{Na}m(t)^3h(t)(V-E_{Na})+g_Kn(t)^4(V-E_K)+g_L(V-V_L)-I_{Ca}(B_{eff},t)=0\ , \qquad (1)$$

where V is the transmembrane voltage, g_i (i =Na, K, L) the channels conductances. m and n are the HH channel excitatory and h inhibitory functions, of microscopic origin not yet well known, although the phenomenological needed powers four, point out to four independent processes, acting for the opening (m, n) and closing (h) of corresponding channels. Leakage channels and voltage/ligand operated ones are probably responsible for the setting of the threshold voltage, V_s but current through them is weak and here neglected. Finally, for our purpose, HH currents have been supplemented by the Ca^{2+} current produced by MF (*HH magnetic* (HHM) equation) as we shall discuss below. We will solve eq.[1] in the *relaxation time, τ, approximation* for the HH functions, where e.g. we assume that

$$dn/dt=-n(t)/\tau_K \qquad (2)$$

where n(t) is assumed to be proportional to the number of K^+-channels which remain closed at time t. Integration of [2] taking t = 0 at the beginning of R process plus H process, yields $n(t)=n_0\exp(-t/\tau_K)$. Similarly taking t = 0 at the beginning of D process we obtain that function $m(t)=m_0\exp(-t/\tau_{Na})$. Otherwise the inhibition function at D process follows the equation $dh/dt=+h(t)/\tau_{inh}$, of integral $h(t)=h_0\exp(+t/\tau_{inh})$. We will now obtain the membrane voltage V (t) dependence, partitioning the impulse in the mentioned regimes.

Repolarization and hyperpolarization: these two processes follow one after other and it is well known that in the R+H process only K^+-channels are open and therefore [1] becomes, $C_m(dV/dt)+g_Kn(t)^4(V-E_K)-I_{Ca}(B_{eff},t)=0$,which integration after substitution of n(t) yields

$$V_K(t)=E_K+(E_{Na}-E_K)\exp\left[-\left(g_Kn_0^4\tau_K/4C_m\right)\left(1-e^{-4t/\tau_K}\right)+\int_0^t dt'\,I_{Ca}(B_{eff},t')/\left(V_K(t')-E_K\right)\right], \qquad (3)$$

which is an integral equation in $V_K(t)$ with kernel $I_{Ca}(B_{eff},t)$. We will show below (from [8] and [10]) that $I_{Ca}(B_{eff},t)=-(N(0)f(B_{eff}=0)q_{Ca}/\tau_{Ca})\exp(-\alpha B_{eff}^2)\exp(-t/\tau_{Ca})$, where N(0) is the initial Ca^{2+} ion number in a burst and τ_{Ca} the Ca^{2+} relaxation time (diffusion time in the cytoplasm) (t origin in [3] is taken at $V(t)=E_{Na}$, origin of R). For comparison with experimental results in single neurons, it is useful to work in frequency domain,ω so that we will obtain the *frequency spectrum* of the spontaneous impulse $V_K(t)$. Fourier transform (FT)

of [3] exp[…] function is unknown, but for $t < \tau_K$ first exponential can be series expanded, so obtaining

$$V_K(t) \approx E_K + (E_{Na} - E_K)\left[1 - \left(g_K n_0^4 \tau_K / 4C_m\right)\left(1 - e^{-4t/\tau_K}\right) + \int_0^t dt' I_{Ca}\left(B_{eff}, t'\right) / \left(V_K\left(t'\right) - E_K\right)\right]. \quad (4)$$

The ω spectrum of [4] *spontaneous* $V_K(t)$ ($I_{Ca} = 0$) is obtained by Fourier transforming $V_K(t)$ around a central frequency ω_0, characteristic of the impulse, yielding (except for a Dirac $\delta\left(\omega - \omega_0^*\right)$ artefact introduced by the exponential series cut-off)

$$V_K(\omega) = A \Big/ \left[\left(\omega - \omega_0\right)^2 + (\Delta\omega/2)^2\right], \quad (5)$$

where $A \equiv g_K n_0^4 \tau_K / 4C_m$ and $\Delta\omega/2 = 2\pi/\tau_K$ the HMHW, which provides τ_K. Therefore the impulse spectrum is the familiar *Lorentzian* function, taking its maximum value at $\omega = \omega_0$. Eqs. [4] and [5] can be easily extended to the real situation of having different types of K^+-channels (up to seven in *Helix aspersa* neurons (Azanza et al., 2008)), but this extension is not very suitable for comparison with the impulse because of the too large number of parameters involved.

Depolarization: this process follows after the refractory time and threshold voltage establishment, and since involved Na^+ channels are operated by voltage, inclusion of Ca^{2+} current sums only a term to $V_{Na}(t)$. But also retarded in time K^+ channels are opened, although being in small number during D tram their current can be neglected. The HHM relevant equation is then $C_m(dV/dt) + g_{Na} m(t)^3 h(t)(V - E_{Na}) - I_{Ca}(B_{eff}, t) = 0$, which in presence of MF yields another integral equation. Integration followed by the first exponential expansion as before yields

$$V_{Na}(t) \approx E_{Na}\left[1 - \left(g_{Na} m_0^3 h_0 \tau_{eff} / 3C_m\right)\exp(-t/\tau_{eff}) + \int_0^t dt' I_{Ca}\left(B_{eff}, t'\right) / \left(V_{Na}\left(t'\right) - E_{Na}\right)\right], \quad (6)$$

where the relaxation time is given by $\tau_{eff}^{-1} = \tau_{Na}^{-1} - \tau_{inh}^{-1}/3$, since the inhibition and activation are independent processes. As before the ω-spectrum of spontaneous $V_{Na}(t)$ is Lorentzian of $\Delta\omega/2 = 2\pi/\tau_{eff}$, and $A \equiv g_{Na} m_0^3 h_0 \tau_{eff} / 3C_m$. Extension to different kinds of Na^+-channels is not worthwhile because of above mentioned reason. Ca^{2+} and Cl^- channels operated by voltage as well would be treated in the same way to Na^+ ones, but as mentioned before their associated currents can be safely neglected.

2. Biophysical experiments.

2.1 Experiments made on single unit neurons from *Helix aspersa* (mollusc) brain ganglia by applying static (SMF) and alternating (ELF) magnetic fields .

Since experiments under low intensity SMF and alternating AC-ELF MF ones are intimately related in their interpretation with the ones carried out under modulated MW fields it is important to present them, in order to fully understand the neuron behaviour under the

latter. We will briefly describe the experimental set-ups for the three kinds of experiments, as follows.

2.1.1 Experimental set-up for exposure to SMF.

Brain ganglia (about 6 mm^3 of volume) (Fig. 4) were placed in the centre of an electromagnet polar pieces (Fig. 5). Nervous ganglia were immersed in molluscs Ringer solution.

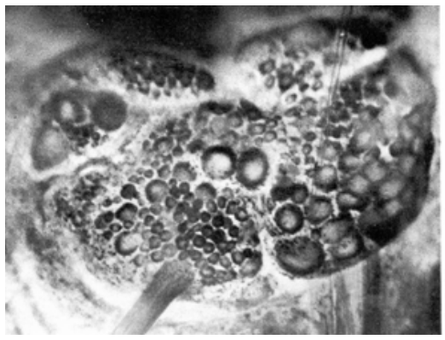

Fig. 4. Microelectrode inside neuron F1. (from Kerkut et al., 1975).

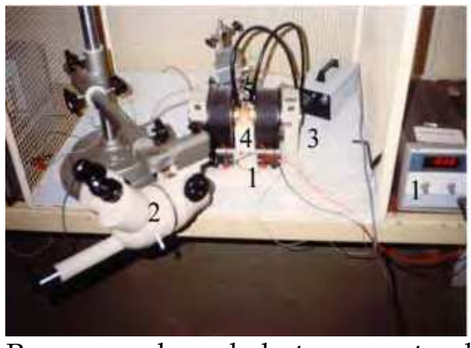

Fig. 5. SMF application. 1: Power supply and electromagnet polar pieces. 2: Microscope. 3: Cold light. 4. Brain ganglia in the centre of polar pieces. 5. Microelectrode.

Intracellular electrophysiological activity from single neurons was recorded in real time with glass microelectrodes (tip diameter < 0.5 μm, tip resistance 2-20 MΩ), filled with a conducting 1M potassium acetate solution (pH 6.8) (Fig.5). Intensities of applied SMF were in the range of 1.0 mT up to 0.7 T (Azanza, 1988; 1989; 1990; Azanza and del Moral, 1994 1995; 1996). Applied MF -either static or alternating- were perpendicular to local geomagnetic field (GMF) lines. Set-up was disposed inside a Faraday cage.

2.1.2 Experimental set-up for exposure to ELF-MF.

Brain ganglia samples, were disposed between a pair of Helmholtz coils as above described for exposure to SMF (Fig. 6). Applied ELF-MF were of: frequencies between 0.1 and 217 Hz and AC amplitude between 0.2 μT up to 15 mT. Experiments at AC, μT amplitude, were performed inside a Mumetal chamber (Fig. 7). The screening was of 100 times, relative to the values of local geomagnetic field (GMF). The AC amplitude inside the Mumetal chamber,

was of 0.1μT with respect to the ambient AC field of 0.2 μT (Azanza and del Moral, 1998; Azanza et al., 2001, 2002; Calvo et al., 1999a, b; Pérez-Bruzón, 2006).

Fig. 6. Experimental set-up for application of ELF-MF. The neuron sample is placed between a pair of Helmholtz coils.

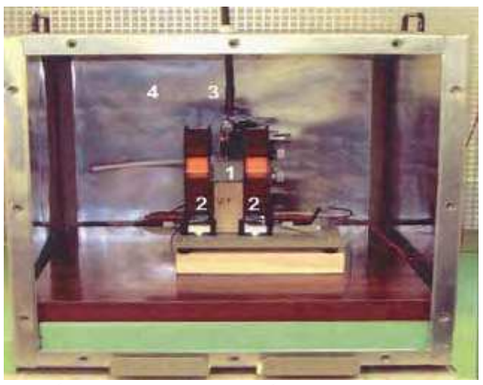

Fig. 7. Exposure to ELF-MF of 0.2 μT, 2μT and 12 μT were performed inside a Mumetal screening chamber (4). (3) Cold light. (2) Helmholtz coils. (1) Brain sample.

2.2 Experiments made on single unit neurons from *Helix aspersa* (mollusc) brain ganglia by applying 13.6 GHz microwaves, modulated by ELF-EMF.

2.2.1 Experimental set-up and dosimetry

Helix aspersa brain ganglia were maintained as described above for SMF and ELF-MF experiments. For exposure to EMF of 13.6 GHz the ganglion bath was placed within a resonant, open, toroidal cavity (Fig. 8). The resonant cavity (Figs. 8 and 9) is made of a 1 mm thickness dielectric ring of FR4, cooper metallized on both surfaces, which are in turn aluminium short-circuited in their external edge for forming the cavity. The MW field was generated by a home made Gunn diode oscillator, which modulates in amplitude the high frequency voltage by an ELF frequency signal voltage between 2-100 Hz. The MW–MF is homogeneous within an area of about 4 mm^2 around the cavity centre, where the ganglion is accurately positioned. The MW EF ($E_0 \cong 3.5$ V/m) is polarized along Oz axis (Figs. 8 and 9) and is homogeneous within the cavity height.

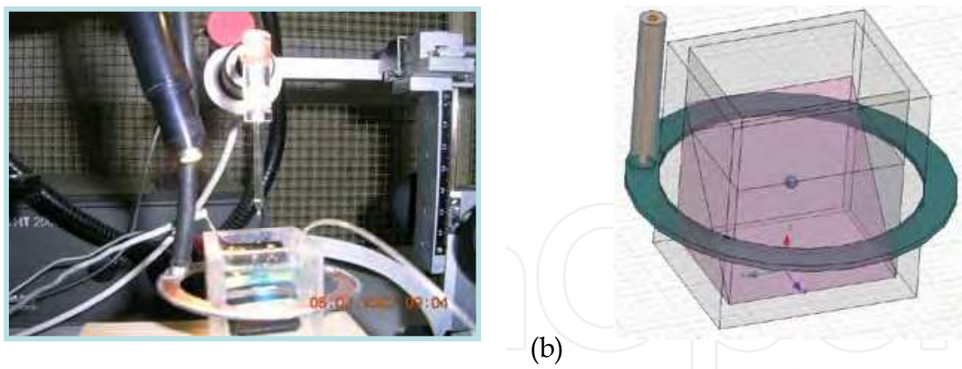

(a) (b)

Fig. 8. (a) Set-up for MW-MF exposure and schematic diagram of the set-up. Nervous ganglion was accurately positioned at the cavity centre, where the field is quite homogeneous. b) Idealized set-up for dosimetry calculations.

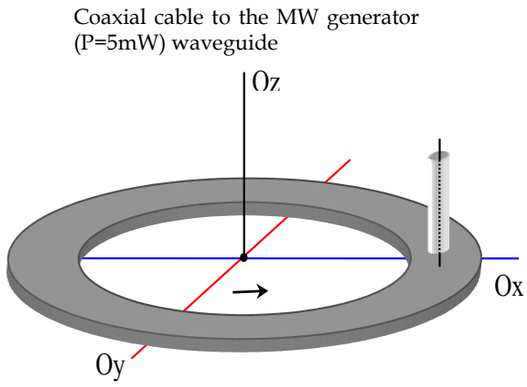

Fig. 9.- Toroidal cavity (mode TEM): external radius r_e = 2.5 cm; internal r_i = 2cm; h=1 mm. Magnetic field **H** is polarized in the cavity plane (the one of the biological sample), along the coaxial cable to the MW generator (P=5mW) waveguide. On Ox axis containing the feeding port. Electric field, **E** is normal to plane.

The MW signal was extracted using a rectangular waveguide, working in a dominant TE_{10} mode, followed by a coaxial cable (50 Ω), so that the mode becomes TEM, the cable being connected to the cavity by BNC gold plated connector. Modulation depth was fixed at 90%. MW frequency of 13.6 GHz was measured using a MW spectrum analyzer E4407B (Agilent) and the generator output power of 5 mW was measured using a power meter 4231A (Boonton). Typical Poynting vector at the cavity center was S ≅ 0.35 W/m². Typical peak value of $H_o \cong 0.10$ Am^{-1} (= 1.25 mOe) at the *Helix* brain ganglia position (cavity centre) (note this intensity is close to the lowest one applied in our ELF alone experiments). The bioelectric impulses were Fourier spectrum analysed using computer standard methods (Chart v 4.1.2 program for Windows, ADInstruments). It is also worthwhile to mention that the applied MF in the electrophysiological experiments was of the same order of magnitude that the applied to astrocytes in our experiments of irradiation performed within the GTEM anechoic chamber (Fig. 21B).

The values of SAR (Fig. 10) and measured temperature increase of sample, between 0.0258 and 0.0261 ^{o}C show that the experiments have been carried out under non thermal conditions. Therefore measurable *thermal effects are not expected.* Dosimetry calculations

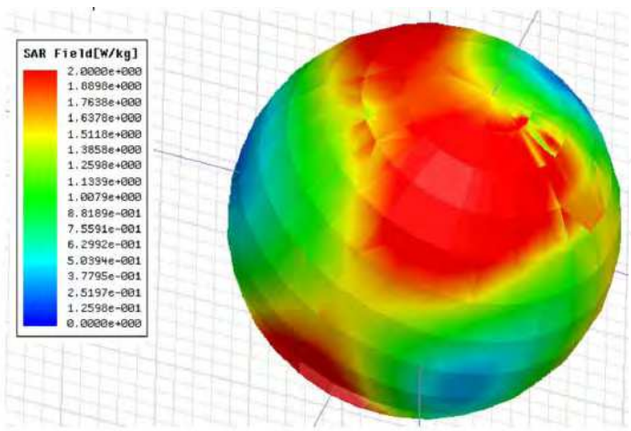

Fig. 10. SAR in the surface of the sphere (nervous ganglion). The mean value of SAR in the volume occupied by the sphere is 2.02x10^{-3} W/Kg.

were made by using the method of finite elements in frequency domain implemented in commercial package ANSOFT HFSS.

Although the open cavity radiates some of the injected electromagnetic power (5 mW) to the exterior it has been shown that it keeps an EMF distribution similar to the closed cavity one (field distribution is only perturbed within the metallic ring). As the chamber with Ringer solution and nervous ganglia is introduced inside the toroid some field attenuation is expected due to the conductivity of the saline solution. Also dominant polarizations in the centre of the applicator are perturbed with respect to the empty applicator. Calculated temperature variations, ΔT, in the Ringer bath solution under applied MW are similar to the values measured with respect to a control Ringer solution not illuminated with MW. The measurements were made with a calibrated R_0 = 100 Ω (0^{o}C) Pt-resistor thermometer (0.01^{o}C precision, resistance temperature coefficient α =0.03.850 x10^{-2} Ω/^{o}C between 0-100^{o}C) and a multimeter (0.0001 ohms resolution) using the four point technique for temperature dependent resistance measurement. Temperature was obtained from linear interpolation, $t=(R_t - R_{0)})/ \alpha R_{0.}$

2.3 Experimental Results

2.3.1 Main experimental observations by application of SMF and ELF (0.1-50 Hz) magnetic fields.

We have observed that the behaviour of an individual neuron, against an applied MF, either static or alternating, is not random but fixed for a mapped neuron: stimulation, decrease of the activity and eventual inhibition and slow response or no response. Magnetic fields, either SMF or ELF-MF, induce effects which reproduce normal, spontaneous, activities of neurons. Applied MF seem to work as switchers, they switch on/switch off the spontaneous activities. Responses of excitation/inhibition are shortened under applied MF.

Under applied SMF, about the 70% of neurons show a Ca^{2+}-dependent modification of the *spikes-frequency* (see spike in Fig. 2), with non appreciable modification of spike shape. For the 50 % of neurons the frequency decreases and eventually are inhibited. For the 20 % of neurons the frequency increases, being stimulated. For the remainder 30 % of neurons very slow or no responses are observed. After long time exposures, spikes-amplitude decrease through a mechanism dependent on the progressive inactivation of the $3Na^{+}$-$2K^{+}$-ATP-ase pump (Azanza and del Moral, 1996). We have observed higher neurons sensitivity under applied ELF-MF. For the 56% of neurons they are inhibited. About the 26% of neurons are stimulated and about 18 % of neurons show slow or no responses. Spikes frequency responses are more frequent than spikes amplitude responses. Also neurons show a much higher sensitivity to frequency variations than to amplitude variations of applied MF (Pérez-Bruzón, 2006).

Searching for the origin of stimulation/inhibition induced effects on neurons, we were able to experimentally show that MF somehow induces the liberation of Ca^{2+} ions in the cytosol. Depending on *neuron type* the increased free cytosolic calcium concentration ($[Ca^{2+}]_i$) produces: i) the increase of neuron membrane conductance for K^{+} ions (g_k) through Ca^{2+}-dependent-K^{+}-channels in turn promotes the sorting out of K^{+} ions to the extracellular fluid, hence the hyperpolarization and so *inhibition* of neuron activity; ii) the increase of positive charge directly induces the Ca^{2+}-dependent-membrane depolarization, promoting in turn the neuron *stimulation.* We have shown *mimic effects* between the induced ones by MF and the induced by increased $[Ca^{2+}]_i$, after a set of key experiments: i) by promoting the entrance of Ca^{2+} ions into the cytoplasm increasing by seven times the Ringer Ca^{2+} concentration (Azanza and del Moral, 1988, 1994); ii) by promoting the liberation of Ca^{2+} ions from the endoplasmic reticulum into the citosol with caffeine –agonist of ryanodine receptors- (Azanza, 1989, 1990; Azanza and del Moral, 1994) and iii) by promoting the entrance of Ca^{2+} into the citosol through NMDA-receptors activated by glutamate (Calvo, 2003; Azanza et al. 2009). The most important conclusion is that *inhibition and stimulation are Ca^{2+}-dependent processes*, neuron-specific and are the result of membrane molecular structure expressed in terms of: kind, localization and relative density of ionic channels in plasma neuron, as we have shown by the characterization of *Helix* channels by immunocytochemistry (Azanza et al. 2008).

Main observations under exposure to ELF-MF were as follows:

2.3.1.1 - Synchronization of at least pairs of neurons activity defined as a *coincidence in spikes frequency and firing rhythm* in time (Azanza et al., 2002, 2009). One of the most striking behaviour was oscillatory and recruitment activities observed after some time under exposure to sinusoidal ELF-MF. These characteristics of neuron activity are the expression of a kind of *synchronizing* activity of neurons relatively far away one each other but integrated in a small network (Fig. 11). Connexin proteins which make *gap* contacts between neuron-neuron and neuron-glia cells are the main responsible for synchronization in mammals brain. In our studies by simultaneously recording the bioelectric activity from pairs of neurons we have observed that synchronization occurs in the 27 % of pairs of neurons studied (Azanza et al., 2002). We have studied the expression of connexin 26 by immunocytochemistry methods and shown that it is expressed in only the 4% of neurons in all the *Helix* suboesophagic ganglia (Azanza et al., 2007). These results plus the comparison of synchronization recordings with the ones mediated by neurotransmitters in synapsis are

a strong support in favour of the participation of MF in the synchronization process (Azanza et al., 2009). The synchronization encompasses clusters of e.g. 7 and 13 neurons, surrounding a central one. The calculated neuron number in the cluster using the model of § 3.2 agrees remarkably with the experimentally inferred number (Azanza et al. 2002).

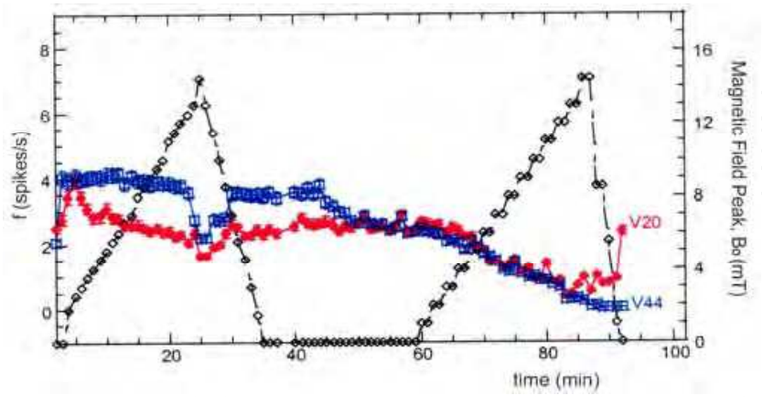

Fig. 11. Experiments were made by simultaneously recording the activity from neuron pair V44 (□, blue) and V20 (♦, red). Under exposure to 50 Hz, 0.5-15 mT EMF (◇), frequency increases reaching the same value in 2 min. As the applied ELF-MF amplitude increases the frequency of V44 did no change, but frequency for V20 goes down to its initial value. For ≈15 mT the frequency decreases sharply in parallel for both neurons, reaching a minimum value. As ELF-MF amplitude decreases the frequency for both neurons increases in parallel reaching the initial, spontaneous, value. At min. 35 the MF is switched off, no changes in the firing frequencies are observed. After 6 min (min. 41), the frequencies for both neurons start approaching, reaching same value at min 50. Synchronizing activity remained for about 32 min., disappearing when the applied field goes down. (Calvo et al., 2002; Calvo 2003).

2.3.1.2 - Frequency window effect: the neuron firing frequency, f , decreases with the applied MF frequency, f_M, as a *Lorentzian*, centred at about the spontaneous, f_0 , one (Figs. 12 and 13) (Pérez-Bruzón et al., 2004; Pérez-Bruzón, 2006; Azanza et al., 2007b).

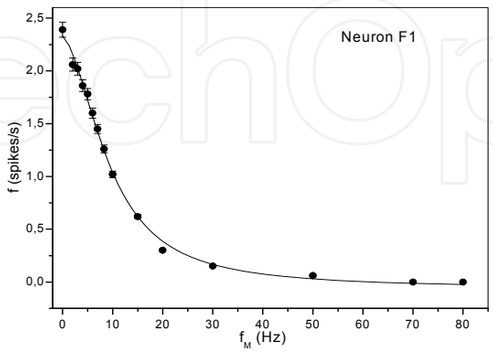

Fig. 12. Neuron F1. Lorentzian (line) fits the variation of neuron f (expressed in spikes/s) vs. field frequency, f_M. f_0=2.5 Hz, $\Delta f_{1/2}$= 9.9 Hz.

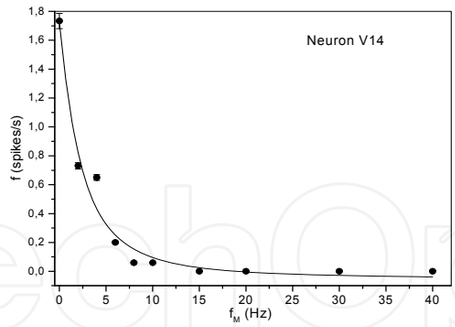

Fig. 13. Neuron V14. Lorentzian (line), fits the variation of neuron *f* (expressed in spikes/s) vs. field frequency, f_M. f_0=2.0 Hz, $\Delta f_{1/2}$= 2.7 Hz.

2.3.1.3 - Resonance effect: we have experimentally shown in molluscan brain single neurons that as the frequency of the applied MF, f_M, was coincident with the main frequency, f_0 of the Fourier spectrum of the spontaneous bioelectric activity voltage impulse, the neuron firing frequency showed a maximum, an effect so called *frequency resonance* (Fig. 14) (Pérez-Bruzón et al., 2004; Pérez-Bruzón, 2006; Azanza et al., 2007b).

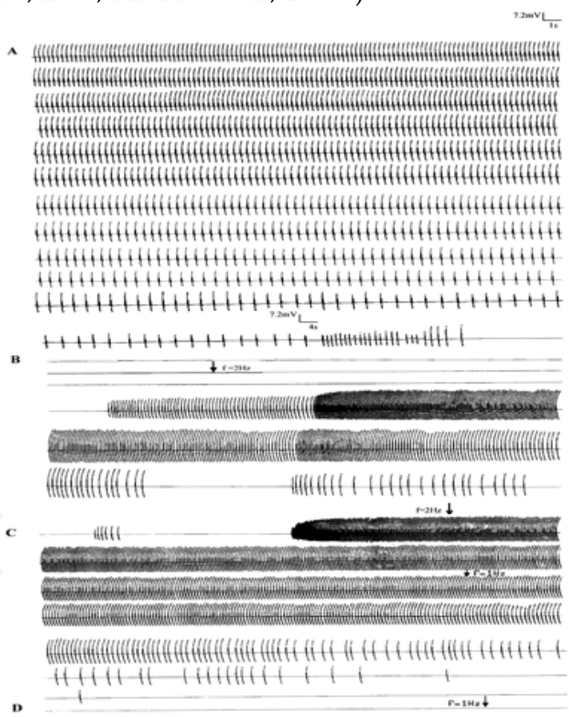

Fig. 14. Neurone V19. **A**): Spontaneous f = 2.4 spikes/s, frequency and amplitude progressively decrease, being the neuron activity completely inhibited after 6 min. of recording. **B**): ELF-MF of 1 mT-2 Hz, was applied for 10 min. With 4 min delay the neuron activity (frequency) was stimulated, spikes amplitude also increasing. C): ELF-MF of 1 mT-2 Hz was applied, the frequency and amplitude increased for a second time. As 1 mT-1 Hz was applied, the neuron frequency was progressively decreasing and neuron activity completely inhibited. Experiment duration: was of (Pérez-Bruzón, 2006).

2.3.1.4 - Demodulation effect: the purpose of our research by applying MW electromagnetic fields (EMF) amplitude modulated (90%) by ELF-EMF was to separate out the possible effect of the MW from the one induced by modulated ELF-EMF within a wider range of frequencies, i.e. 2-100 Hz.

The exposure of neurons to MW modulated by ELF-MF MF between 2 and 20 Hz and 20 Hz have shown that are the ELF-MF the responsible for the elicited responses (Figs. 15a and 16), a so called *demodulation effect*. Main observation was *no effect under the carrier*, f_c=13.6 GHz, but "*frequency resonances" at low frequencies*, e.g. f_M =16 Hz (Figs. 15a, 16), similar to the case of only ELF application, i.e. also with *Lorentzian profiles* (Fig. 17) (Azanza et al., 2007b; del Moral et al., 2008). The effect is a "*frequency resonance"* of *Lorentzian* shape, when the *MF frequency matches the characteristic frequency (-ies) of the neurone impulse Fourier spectrum* (Figs. 15b and 18b). We should stress that a *"frequency resonance"* is a maximum in the spectrum $f = f(f_M)$, where f is the bioelectric or spike frequency repetition. In neuron V14 two frequency resonances are observed at f_M = 4 and 16 Hz (Fig. 16). On Fig. 17 we can see *Lorentzian* fits to the f_M = 4 and 16 Hz resonances in neuron V14 (Fig. 16). As we will see this is an important observation upon which to base the model proposed in § 3.4 for the effect of ELF amplitude modulated MW upon neuron bioelectric activity. Note that the resonance observed in *not* an amplitude one ("spring" resonance).

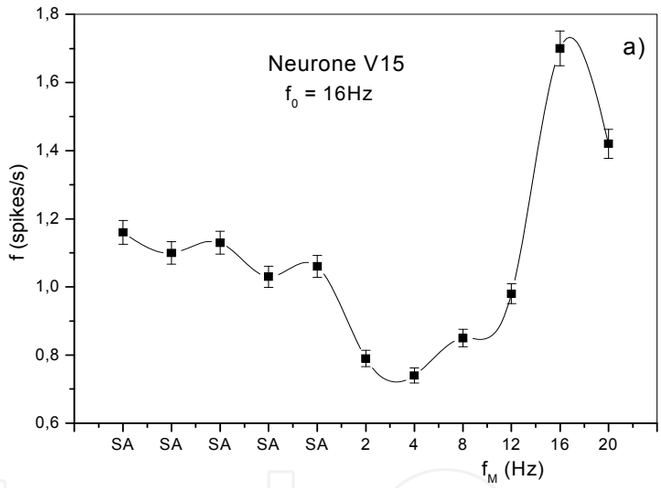

Fig. 15. a) SA, spontaneous activity. The carrier was modulated at 2, 4, 8, 12, 16, 20 Hz. Neuron V15 shows a *resonance* effect at 16 Hz. b) Spontaneous activity Fourier spectrum gives a maximum for 16.4 Hz.

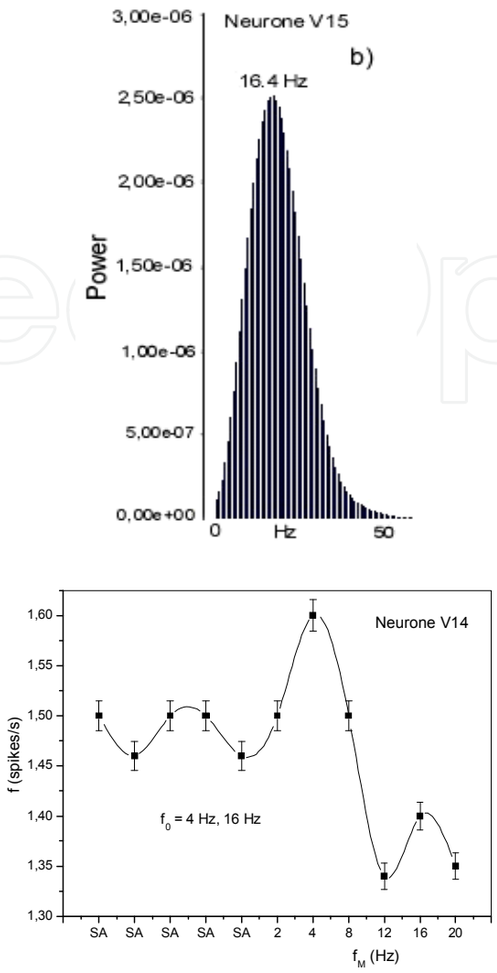

Fig. 16. Frequency *resonance* effect showing maxima at 4 and 16 Hz from neuron V14: frequency window effect.

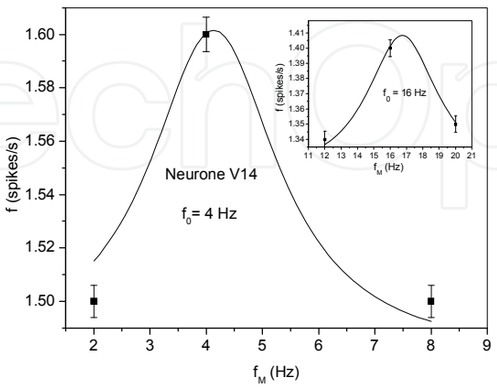

Fig. 17. Lorentzian fits (continuous line) to the resonances shown in Fig 16. The HMHWs are respectively 1.4 and 1.6 Hz.

The resonance effect seems to be neuron specific. In the experiment on neuron F32 (Fig. 18a), caffeine (3mM) does not induce any Ca^{2+}-dependent activity (Azanza, 1989). When Ringer solution is added in order to remove caffeine, we observe a small increment in neurone bioelectric activity. This increment is not relevant from the statistical point of view. MW carrier alone (C) was applied and then the carrier modulated by ELF from 2 to 100 Hz frequencies. *Resonances* at 4 Hz and 50 Hz are observed. Fourier spectrum (Fig. 18b) gives a maximum for 4.2 Hz which is coincident with a maximum neurone frequency (4 Hz) (Fig. 18a). Resonances at 12 and 50 Hz are observed for other kinds of neurons (Fig. 19).

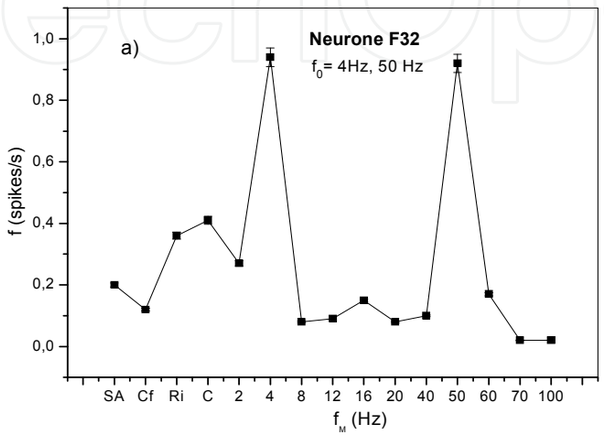

Fig. 18a. SA, spontaneous activity. Cf, caffeine. Ri, Ringer solution. C, MW carrier, induces a non significant modification of bioelectric activity. *Resonances* at 4 Hz and 50 Hz are observed.

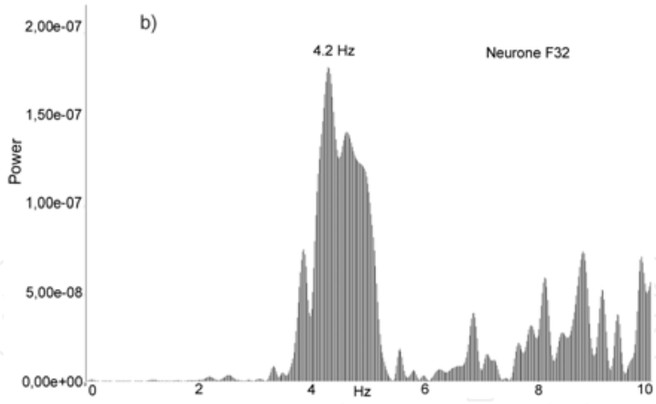

Fig. 18b. Fourier spectrum give one maximun value at 4.2 Hz which is coincident with maximum neurone frequency. A filter to avoid 50Hz noise prevents getting the correspondent maximum.

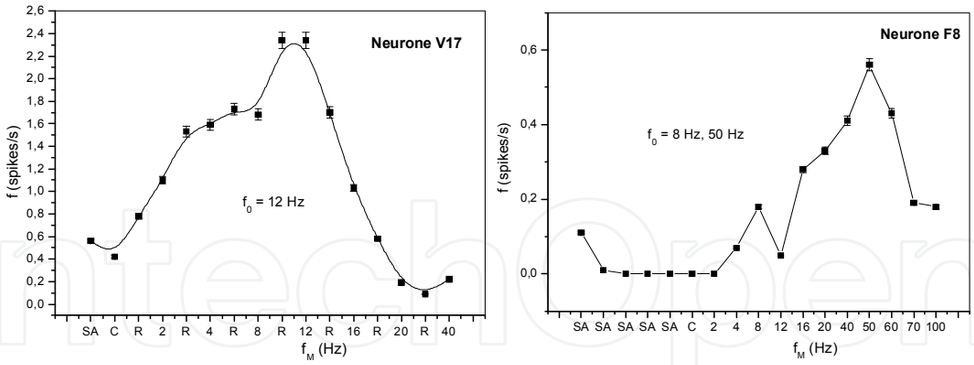

Fig. 19. Resonances at 12 Hz (neuron V17) and 8 and 50 Hz (Neuron F8).

Two conclusions can be summarized from the above experiments:

i) Neurone plasma membrane (see § 3.4) seems to behave as a physical system able to resonate as the MF frequency matches some characteristic one of the bioelectric impulse other than the spontaneous neurone frequency (Azanza et al., 2007b). An approach has been made for the interpretation of our resonance results consistent in a membrane depolarization due to the increase of cytosolic Ca^{2+} concentration. Ca^{2+} is detached from plasma neurone membrane through the superdiamagnetism (SD) and Ca^{2+} Coulomb explosion (CE) as explained in § 3.4 (del Moral and Azanza, 1992; Azanza and del Moral, 1994).
ii) Neurone bioelectric activity is highly sensitive to *low frequency* applied alternating MF modulating a MW carrier in the ten of GHz range. *Extremely low frequency modulated MW radiation* at non-thermal level of field power density (ΔT increase in bath lower than $0.01^{o}C$) modifies neurons bioelectric firing frequency, in a *resonant* way. The *resonance* appears when the ELF applied MF is close to a characteristic *frequency of the impulse train Fourier spectrum* (*not* to the firing frequency, del Moral et al., 2008).
Stimulatory effects by MW modulated by ELF-EMF have been described on human volunteers electroencephalogram recordings (EEG). 400 MHz 100 % modulated in the EEG physiological spectrum, at frequencies of 7, 14 and 21 Hz showed increased alpha (8-13 Hz), and beta (13-30 Hz) rhythms. Alpha and beta rhythms were also activated by MW modulation at 40 Hz and 70 Hz (Hinrikus et al., 2005). Similarly to observations on humans EEG we have got resonances at frequencies in the alpha and beta rhythms, values much higher than the spontaneous *Helix* neurons frequency (0.1-8.0 spikes/s). Our conclusion is that the *frequency resonant effect* must be the expression of an intrinsic biophysical property common to molluscan and human plasma *membrane* neurons which appears when the ELF applied MF is close to a *characteristic frequency of the bioelectric impulse train Fourier spectrum*. These observations could explain the effects observed on human EEG.

2.4 Experiments made on astrocytes from human astrocytoma tumour submitted to 9.6 GHz amplitude modulated by low power ELF-MF of 100 and 800 Hz.

Another kind of experiments has been performed consisting in the study of glia cell (human astrocytes) proliferation process under also ELF amplitude modulated MW EMF, that we

will briefly discuss. The underlying mechanism to explain them may be also the Ca^{2+} detaching from membranes.

Brain neurons and astrocytes are cells of crucial interest for the research of potential effects of MW produced by communication systems. Astrocytes are a physical support for neurons in human brain; they feed neurons by supplying metabolites from blood; they provide a neurotransmitters and ions buffer system to the brain, and with endothelial brain vessels membrane makes the *blood brain barrier* (BBB) and are able to proliferate, being the responsible for more than 90% of human cellular brain tumours (gliomas). Any modification in any of their activities will potentially produce negative effects on brain function and human health.

The aim of our work has been to characterise the effects of short MW pulses upon the physiology of astrocytes in culture by means of cellular and biochemical studies trying to characterize any possible toxic effect by comparing the results obtained on non-exposed, standard sham-control conditions, with the ones obtained under exposure to MW.

2.4.1 Experimental set-up and dosimetry.

Experiments were performed on astrocytes from human astrocytoma (Clonetics line 1321N1). Cells were maintained in culture as an adherent monolayer in a humidified atmosphere of 5% CO_2 at 37ºC in a standard incubator. After 6 days cultured, cells were transferred to the GTEM-incubator for exposure to MW inside a horn shape GTEM cell, where the TEM radiated MW is from a flat strip line along a border. MW were produced with a solid state MW generator (100 KHz-20 GHz range), provided with a versatile modulator of different wave profiles (modulation depth 90%), followed by a high power (50W maximum output) MW travelling-wave tube amplifier, followed by a directional coupler, which injects the MW signal into the GTEM chamber through a 50 ohm coaxial cable (Fig. 20). ELF modulation was kept for all irradiations at 90%. Direct and reflected from chamber powers were monitorized via a diode bridge. GTEM chamber is provided with anechoic walls to reduce unwanted reflections. The EMF-MW mode was the TEM one, same as usually in wireless telecommunication.

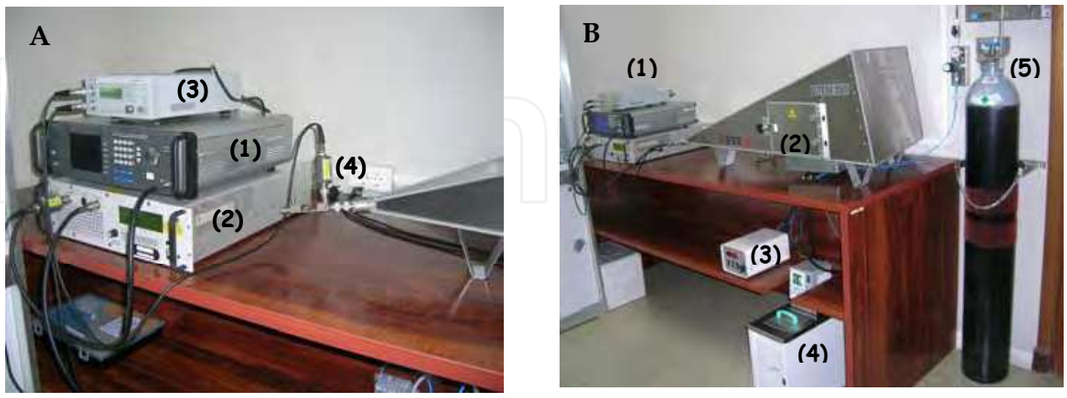

Fig. 20. **A**. (1) Microwave generator (GIGATRONICS 2520A). (2) Medium Power Wide band amplifier (T186-50). (3) RF Power meter (BOONTON 51013). (4) Directional coupler: frequency range: 4-18GHz (COU-BD418 G 50W-35). **B**. (1) Electronic equipment connected to the GTEM - Cell (2). Olympus - incubator regulators: (3) CO_2 regulator; (4) Temperature regulator; (5) CO_2 container.

Two cells culture flaks were placed into the GTEM-cell where the EMF is rather homogeneous, with their longitudinal axis in the same direction of EM wave incidence. In Fig. 21 are shown the simulation layout for the dosimetry calculation for the whole system and SAR calculation along an observation line at 50 μm height from the bottom of the flask (the estimated cell layer thickness). EF calculated values were: 0.05-0.25 and 0.10- 0.35 V/m for the two flaks respectively. The calculated MF were: 4.6-8.8 A/m, and 4.8-9.1 A/m for the two flaks. MF and EF intensities measured, are of the same order of magnitude to the ones that we are applying in our electrophysiology studies on neurons. The EF was normal to the plane of the cells monolayer and the incident MF in the horizontal plane of the monolayer. Calculated temperature increases due to MW power exposure were below $3x10^{-5}$ ^{o}C. *Therefore we can assume negligible thermal effects in the cells* (for detailed descriptions of dosimetry see Pérez-Bruzón et al., 2009).

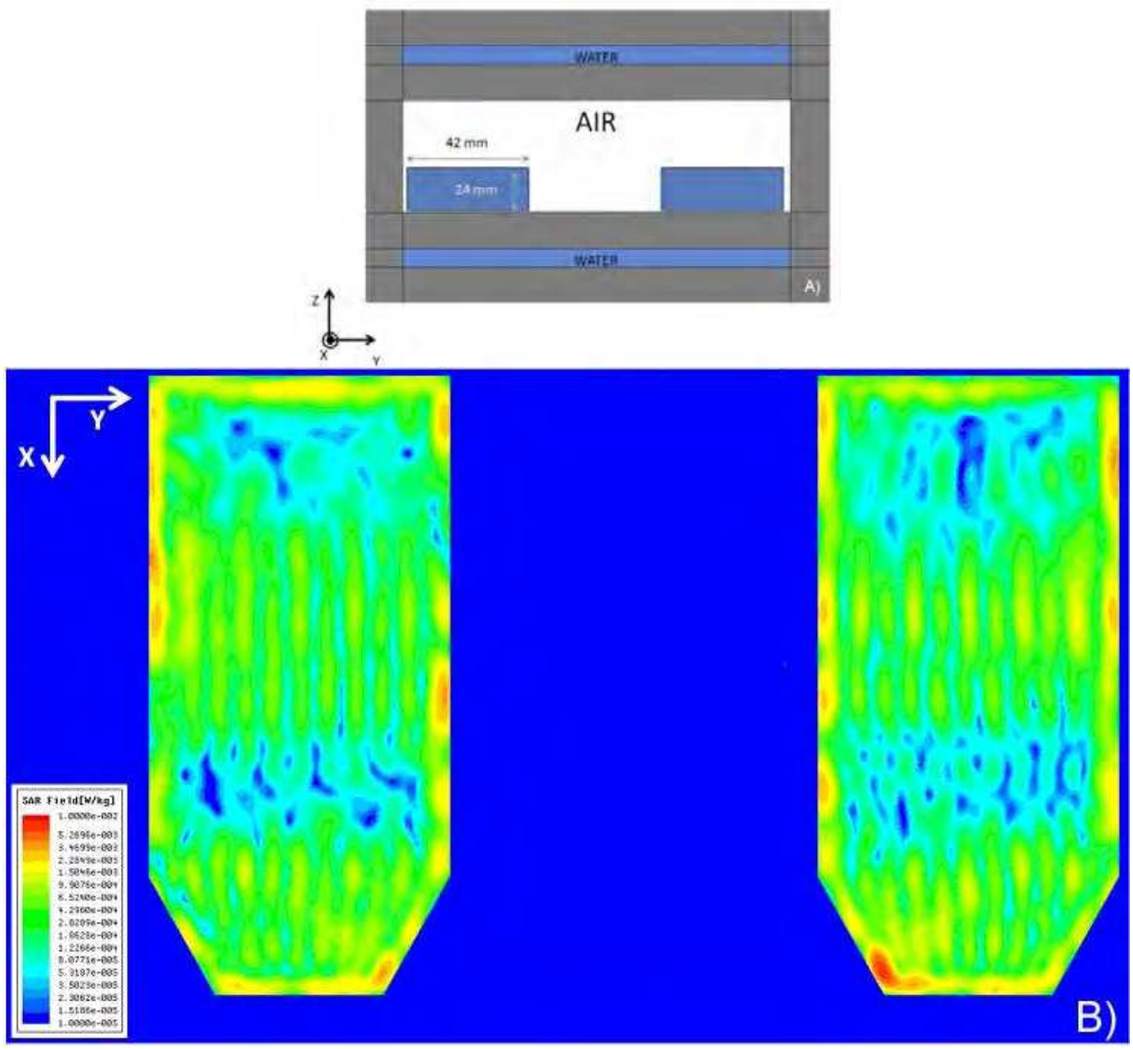

Fig. 21. **A)** Transversal section of 2 Falcon flasks inside the GTEM- incubator system. **B)** SAR simulation in a plane at 50 μm height from incubator base. The mean SAR value from left to right was $3.99x10^{-4}$ W/Kg and $4.08x10^{-4}$ W/Kg (incidence direction +X).

2.4.2 Experimental results

In our experiments we have observed an statistics significant *increased* cell proliferation rate *of about 43%* under 24h exposure to pulsed MW in two experimental conditions: 9.6 GHz carrier frequency, pulse width 100 and 120 ns, pulse repetition frequency 100 and 800 Hz, pulse repetition interval, 1.25 and 10 ms, power 0.34 and 0.60 mW, EF strength 1.25 and 1.64 V/m, MF strength 3.3×10^{-3} A/m (41.4 μOe) and 4.35×10^{-3} A/m (54.6 μOe). Searching for biomarker proteins of astrocytes cell cycle and apoptosis, we found that Hsp-70 and Bcl-2 antiapoptotic proteins were expressed in control and treated samples while an increased expression for connexin 43 proteins was found in exposed samples.

These results open the Ca^{2+} pathway for an explanation of *increased proliferation*. Signal cascade of astrocyte apoptosis may enclose modifications of intracellular calcium concentration ($[Ca^{2+}]_i$), an interesting confluence of molecular pathways to explain the effects under exposure to EMF in two kind of cells of the nervous system: of nervous: neurons and astrocytes. By considering the mechanisms that initiate cell cycle reactions, the induction of cell *stress* could be related to an increased release of hsp (heat-shock) proteins, which need not to be induced by heat production only. Hsps proteins play a critical role in the regulation of the cell cycle, proliferation and apoptosis. The synthesis of Hsp can be produced under several stress conditions: alcohol, oxidative stress, osmotic pressure change, toxic chemicals and exposure to low-frequency EMF (Pipkin et al., 1999; Leszczynski et al., 2002). Our future research will be devoted to study the quantification of Hsp-70, Bcl-2 and Cx43 proteins, in control and irradiated samples, possible increased $[Ca^{2+}]_i$ concentration process and the implication of the anti-apoptotic increase of Bcl-2 protein promoting cell survival (Takuma et al., 2004).

3. Biophysical models.

3.1 Cell membrane as target for electromagnetic field interactions.

The EMF, in the frequency range we are applying, i.e. ELF of 0.1-217 Hz, and 100 and 800 Hz modulating MW carrier and, MW of 9.6 and 13.6 GHz, of low power (SAR induced on biological samples of 4.00×10^{-1} mW/Kg and 2.02×10^{-3} W/Kg respectively), do not posses sufficient EM-energy density to cause ionization (as in the X-ray, U.V and γ ranges of the EM spectrum) or appreciable thermal effects (see dosimetry data). In fact in the range of ELF, the heating effects are eventually due to the production of eddy currents and to the water dielectric relaxation, mainly of α-type, operating at frequencies between ≈ 0 Hz and ≈ 100 Hz (see Azanza and del Moral, 2004 for details). According to the Poynting theorem the maximum average EM energy deposition (i.e. without radiation losses) in a living system is limited by the time average EM density energy, i.e.

$$e_m = \frac{1}{2}\left[\varepsilon H_{rms}^2 + \mu H_{rms}^2\right] \tag{7}$$

where E_{rms} is the EF and H_{rms} the MF r.m.s intensities respectively, and ε and μ, the dielectric constant and magnetic permeability of the biological medium, respectively. Then for an ELF field with a MF amplitude of say ≈ 0.3% Oe, $e_m \approx 2 \times 10^{-15}$ eV/m^3, and e.g. for a neurone of *Helix aspersa*, with diameter ≈ 100 μm, this means that the energy available to the entire cell is only of ≈ 3×10^{-3} eV if whole energy were deposited in the cell. This energy is really negligible either against the atomic ionization energy for the whole cell atoms (of the order of 10 eV/atom, the Van der Waals binding energies of ≈ 0.06 eV/molecule or the

hydrogen bond energies of ≈ 0.16 eV/molecule), or the specific heat (1cal/mole K) for the water within the cell, to produce any noticeable thermal effects (the above energy is around 10^{-8} times smaller than that needed one to rise the temperature of the cell by 1K at room temperature).

An ELF-EMF, both through the EF and through the MF by means of the Faraday induction effect, will produce electric currents in the ionic aqueous solution surrounding the cell. However, the cell membrane is a strong dielectric ($\varepsilon_r \approx 6$) barrier for the passage of those currents to the intracellular medium, except for a small reduced fraction. Therefore if the ELF-EMFs have to produce any effects inside the living cells perhaps they must be through subtle alterations at the membrane level which in turn should convey signals across the membrane body to produce any eventual biochemical and physiological response. The unique characteristics of biological membranes make them the first candidates when searching for EMF interaction sites. Membranes from specialized cells couple the stimuli, carried out by chemical mediators as hormones and neurotransmitters, with the cytosolic machinery inducing in turn physiological responses. Those transduction complexes enclose specific receptor proteins, transductive proteins (i.e. G-proteins) and enzymes (i.e. adenylate cyclase or phospolipase C), which enormously amplify the initial weak impact promoted by the binding of the signalling molecules to their specific receptors. In this sense we can talk about the cell membranes as powerful "amplifiers" of electrochemical or biochemical events occurring in their surroundings. As a consequence of the chemical mediator- receptor interaction, effector molecules at cytosolic levels are triggered -the so called "second messengers"- inducing in turn specific metabolic changes. The best known second messenger molecules are: cyclic-adenosine-monophosphate (cAMP) (Sutherland, 1972); diacylglycerol and inositol trisphosphate (Downes, 1983; Berridge and Irvine, 1984; Nishizuka, 1984); Ca^{2+} ions, central to our model presented in § 3.4 (Nahorski, 1988; Eberhard and Holz, 1988); arachidonate (Irvine, 1982; Loeb and Gross, 1986; Axelrod et al., 1988) and free fatty acids (Ordway et al., 1991).

Therefore in considering the mechanisms of interaction between ELF-EMF and cell membranes we have to take into account the possibility of a direct effect of ELF-EMF on receptor- and transductive-proteins and enzymes and interaction mechanisms. We cannot ignore either the phospholipid bilayer, which mainly constitutes the physical support of the membrane or the glycocalyx, which is an extracellular plasma membrane component essential in the interactions between the cell and its extracellular surroundings. Same can be said about the *inner* surface molecules, which capture free positive ions, e. g. Ca^{2+}.

Non-linear-non-equilibrium processes have been considered as essential ones, at critical steps in the transmembrane signal coupling (Adey 1986, 1988 a, b), for the "*amplification*" of the weak EM energy conveyed by the ELF-EMF interacting with the plasma membrane in order to produce e.g. Ca^{2+} liberation from their membrane stores (as discussed in § 3.4) (del Moral and Azanza, 1992). The mechanism here proposed actually is not an energy amplification *one but nevertheless a cooperative* mechanism within PP clusters (see below). The assumption of having the cell membrane in a non-equilibrium or metastable state of potential energy provides for the possibility that a weak energy EMF stimulus can produce a significant perturbation of the membrane. On the other hand a physical or physicochemical non-linear "device" produces upon a "small" input signal S_i, a sort of amplification giving as output a "small" signal $S_0 = GS_i$, with G>1 only if the "characteristic" curve output vs input is non-linear (Bleaney and Bleaney, 1965). However, an alternative or concomitant way for

amplification is *cooperativism* among the molecular components of the membrane surface. Through a cooperative mechanism, the release of ELF-EM energy at a point in the membrane can be enlarged by the interaction of such a point with another one receiving the released energy and feeding back to the first point part of such energy output plus the one received by itself, within a closed-cycle loop (feedback). It is worthwhile to say that studies on the electrical properties of the squid giant axon (Cole and Curtis, 1939), which led to the well-known Hodgkin-Huxley equations, already showed clearly the non-linear characteristics of excitable biological membranes (Hodgkin and Huxley, 1952).

We should also clearly distinguish between two different ways of interpreting the action of EMF on cell membranes: through the *electric* field action or through the *magnetic* one, although when this is *time varying* (EMF), most theories attach cell effects to the electric one, directly impressed by the EMF and the one induced by the accompanying time-dependent MF (Faraday induction). Nevertheless it is noteworthy that when applying EMF of ELF to cells and tissues, the devices used to apply the quasistationary fields are such that the field is an electric one, except for few cases where the EMF was applied with coils, fed by AC currents, and then it is only when we can talk about the application of a quasistationary MF. In either situation the accompanying field, magnetic in the former case and electric in the latter, is negligible.

We have experimentally shown that increased free *intracellular* Ca^{2+} ions concentration promoted under static (Azanza and del Moral, 1994) and ELF-MF (Pérez-Bruzón et al., 2004) induces modification of the bioelectric activity on neurons. MF of the order of magnitude used in our experiments (≈ 1mT-0.7 T in experiments applying static MF and 0.2 μT-15 mT in experiments applying ELF-MF) are incapable of opening Ca^{2+}-membrane channels or producing by ionization the liberation of Ca^{2+} from the binding sites on the neurone membrane. Nevertheless if we consider the combined effect of *superdiamagnetism* and *Coulomb explosion* upon Ca^{2+} ions, they can be liberated on both *sides* of the membrane (del Moral and Azanza, 1992). The model is based upon the strong repulsion that the Ca^{2+} ions, attached to both sides of the membrane phospholipids (Fig.1), suffer when the *nearest neighbour* (*N.N.*) *opposite* extremes of such diamagnetic dipoles (Fig.22) come close enough to suffer Coulombic repulsion forces with a energy higher than the ionic binding energy to the membrane surface, ε_b. According to the described membrane structure, such electrostatic interaction can only occur between PS-GL pairs. These charged heads are immersed in water with a very high dielectric constant ($\varepsilon_r \cong 80$), giving to this structure low electrostatic repulsive energy, and therefore great stability at its ground state (GS), i.e. without EMF application or against thermal fluctuations.

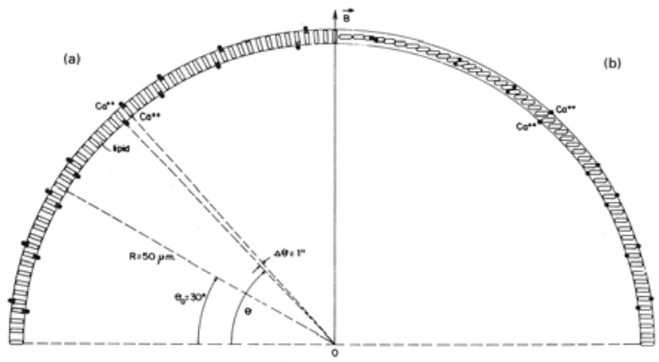

Fig. 22. (a) Schematic layout (not at scale) for the neuron membrane model, showing the lipid molecules (sticks). Some (N.N.)PP (≅ 2% in our model), with attached Ca^{2+} ions are shown. The direction of the applied MF ***B***, as well as the polar angle,θ, of the radial PP molecules phospholipids (PP) molecules molecules and the angle θ_0 below which there is not possible Ca^{2+} liberation are also shown. (b) The same membrane under an applied magnetic field **B**, where diamagnetic PP have fully rotated becoming with their long axes orthogonal to ***B*** and the Ca^{2+} charged heads approach, for a field stronger than a saturation one, B_0 (Azanza and del Moral, 1994).

3.2 Superdiamagnetism (SD) and Ca^{2+} coulomb explosion (CE) model under AC magnetic fields.

This model has been widely tested in single neurons and simple neurone networks under static and ELF MF respectively, where in the latter the MF also induces a *synchronized* bioelectric activity within those networks, as mentioned before (Azanza et al. 2002; Azanza et al., 2005).

The model explains well the neuron bioelectric activity inhibition, i.e. the decrease of firing frequency under applied MF due to Ca^{2+} ions liberation from inner membrane surface. Neuron excitation under applied MF is also thought to be due to increase of Ca^{2+} in the cytosol, that increases the voltage difference across membrane and opens the voltage operated Na^+ (and Ca^{2+} too) channels, giving rise to depolarization, due to the entrance of such ions. The model inhibition contemplates three ingredients: i) The anisotropy of the diamagnetic susceptibility tensor components, $\tilde{\chi}$ (< 0) of the long PP "rods", or difference $\Delta\chi = \chi_{\parallel} - \chi_{\perp}$, between the directions parallel (||) and perpendicular ($\perp$) to the PP axis (the same applies for protein channels). ii) The well proved cluster formation in the membrane liquid crystal of *correlated* PP long axes through their electric quadrupolar moments, $\tilde{Q}_i$ interaction, of pair (i, j) correlation function $C_Q = <\tilde{Q}_i\tilde{Q}_j> - <\tilde{Q}_i><\tilde{Q}_j>$, by

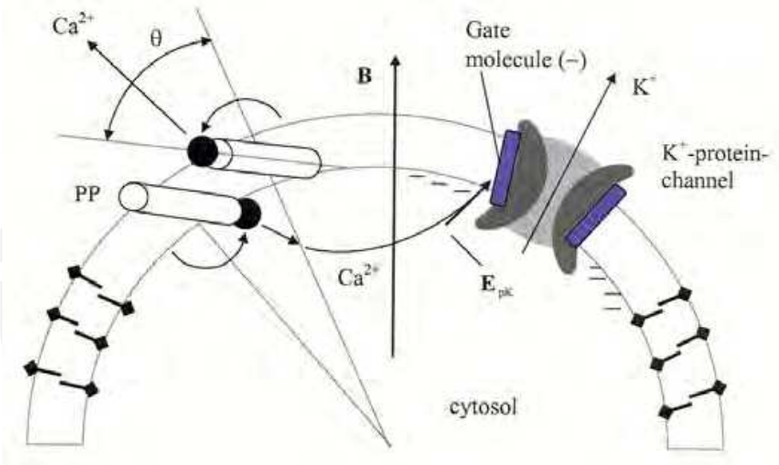

Fig. 23. Two nearest-neighbour Ca^{2+}-charged phospholipids (rods) rotate under their assumed opposite magnetic torques, approaching the Ca^{2+} ions (black circles), attached to the PP negatively charged heads (lozenges). The ions become simultaneously detached from the membrane surfaces when their weak ionic bonds to the heads are broken due to Ca^{2+}-Ca^{2+} Coulomb repulsion. Within the cytosol the Ca^{2+} ions diffuse towards the K^+-protein channels, which are opened when Ca^{2+} is captured (within the Debye shielding length, λ_D) by the "gate" molecule (calmodulin), giving rise to the K^+ outwards current (hyperpolarization) (del Moral et al., 2008).

which the PPs *cooperatively* rotate out from the MF **B** axis (PP electric dipolar moment is very weak). $\langle ... \rangle$ is the ensemble thermal average. The correlation length, ξ usually exceeds a single neurone, *via* the PPs of the interposed glia membranes between neurons, and through the gap junctions (Azanza et al. 2007a). This phenomenon is called *superdiamagnetism* (SD). iii) When the Ca^{2+} ions attached to their PP bilayer inner and outer binding sites (polar heads) happen to be nearest-neighbours (NN, in number N_{nn} per cluster face, with estimated $N_{nn} \cong 0.007 N_c$, N_c being the PP number per cluster), and the NN PPs suffer opposite (with clearly 1/2 probability) magnetic torques $\boldsymbol{\tau}_m = \pm \mathbf{m} \times \mathbf{B}$, the weak ionic bindings are broken by their mutual Coulomb repulsion, of energy ε_{coul}. This produces a *simultaneous* detaching (*Coulomb explosion*, *CE*) of Ca^{2+} pairs (Fig.23 for a view of the mechanisms involved). Note that the Ca^{2+} water solvating and dielectric membrane negative electric images formation reduce the Ca^{2+} effective charge) (for more details see Azanza and del Moral, 1994; del Moral et al. 2008).

The main result from the SD-CE model is the *field intensity dependence* of the neurone bioelectric frequency, $f(B_{eff}, T)$. This frequency is controlled by chemistry mass action law between Ca^{2+} and membrane binder radical, R^- (sialic acid outside and phosphatidylserine inside), i.e. $[Ca^{2+}][R^-] = k(T, B_{eff})[CaR]$, where k is the kinetics constant. Thus $f \propto [R^-]$ becomes inversely proportional to the number of Ca^{2+} ions detached per cluster, $N^c_{Ca^{2+}} = N_{nn} \exp(-\Delta E_c / k_B T)$, where $\Delta E_c(\theta) = -(N_c \varepsilon_m + N_{nn} \varepsilon_{coul})$ is the *dynamic* Peierls's energy barrier (i.e. changing with the PP rotation) to be overcome by the Ca^{2+} ion in order for the PP to steadily rotate. Moreover under AC MF the cell impulse H process (where the cytosol

becomes more negative due the K^+ ions sorting out, Fig.2) is modified by the Ca^{2+} ions (in number of four) binding to the K^+ protein-channel (more specifically to the calmodulin "gate" molecule) and opening it due to the calmodulin electrical unfolding (Babu et al., 1985). Therefore it should be $f \propto 1/N_{Ca^{2+}}$, to first order. Summing now $N^c_{Ca^{2+}}$ from all the PP clusters in membrane(s), the final result is that the neurone bioelectric frequency varies with the RMS MF as

$$f(B_{eff}, T) = f(0, T)\exp(-\alpha B_{eff}^2), \quad (8)$$

where $\mathbf{f(0,T)}$ is the *spontaneous* frequency and the important parameter model $\alpha = N_c|\chi_\perp|V/2\mu_0 k_B T$, that encompasses the PP cluster physical properties and membrane temperature, T, and allows the experimental determination of N_c, or PP number in a membrane(s) cluster (del Moral and Azanza 1992; Azanza and del Moral 1994). As mentioned before for ELF AC MF (quasistatic) we have introduced in [8] the RMS B_{eff}, since magnetic energy density stored in the membrane is $B(t)^2/2\mu_0$, of time average $B_{eff}^2/2\mu_0$. Eq.[8] has been widely and firmly tested in single neurons of *Helix aspersa* for static (del Moral and Azanza 1992) and ELF weak MF (Azanza and del Moral 1998) and for temperature, T modification (Pérez-Bruzón, 2006). The exponential law [8] has been tested for *static* MF application and in Fig. 24 we plot the logarithm of *f* against B^2 for several mapped neurons, for B between 0 and 0.7 T and where we distinguish two linear regimes, with different slopes, due to the different N_c (at the higher fields the clusters are likely fractured and N_c decreases). If we assume $N_c = 5 \times 10^6$ PP/cluster (as deduced from SQUID magnetization measurements in erythrocyte membranes (Azanza et al., 1993)) we obtain a value of $\chi_\perp$ rather close to the measured value, giving good selfconsistence to the model (Azanza and del Moral, 1994). Note that at a critical field all activity is abolished through a first order transition. Now for weak ELF MF the observed firing frequency, *f*, in *Helix* neurons follows a dependence $f(B_{eff}) \cong f(0)(1 - \alpha B_{eff}^2)$, which precisely is the obtained one by performing a series expansion of [8] for $\alpha B_{eff}^2 << 1$ (Azanza and del Moral., 1996).

Regarding to *f* (T) dependence, observations in mapped *Helix* neuron F47 show that *f* first decreases with increasing T at fixed B_{eff}, in disagreement with eq.[8] (see Fig.25). The reason is that those neurons belong to the $\approx 26\%$ of studied ones where *f increases* with increasing

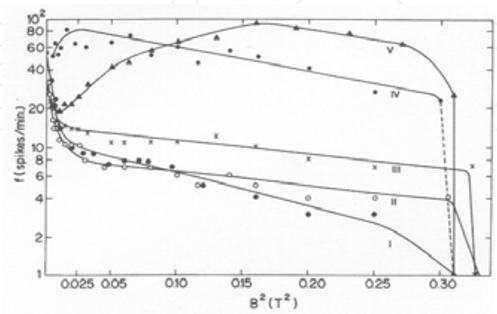

Fig. 24. The logarithm of the firing frequency for several *Helix* neurons vs. the square of the applied magnetic field, **B**. The slope of the linear portions gives $\alpha = N_c V|\chi_\perp|/2\mu_0 k_B T$, with Nc underlying a sudden change at ≈ 0.05T (Azanza and del Moral, 1994).

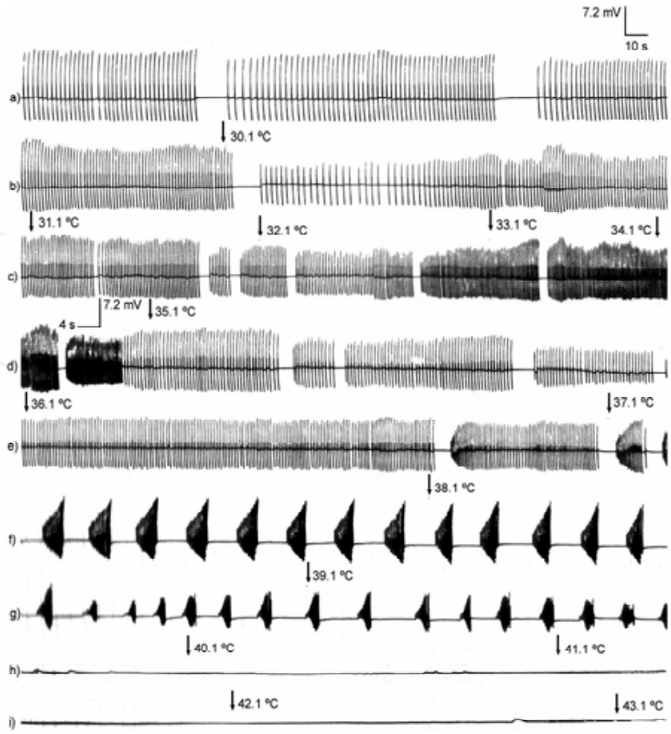

Fig. 25. Temperature effect for neurone F47 bioelectric activity. Transitions at 30ºC and 37ºC within the membrane liquid crystal are observed.

B_{eff} (Azanza and del Moral 1994). The responsible mechanism is that the by MF detached Ca^{2+} ions depolarize the membrane, cytosol becoming more positive, so opening Na^+ and/or Ca^{2+} channels operated by voltage (bioelectric activity *stimulation* mechanism). Also D amplitude V_d *decreases*, the calculated variation in V_d being $\Delta V_d(B_{eff}) = -(4\pi/N_c)E_p \exp(+\alpha B_{eff}^2)$, where E_p is the pump e.m.f., due to opposite to PP protein pump rotation (since $|\chi_\parallel| < |\chi_\perp|$), where PP partially hidden the protein pump, desactiving it (Azanza and del Moral 1996) (see Fig. 26). Also observed are two transitions in the form of increasing

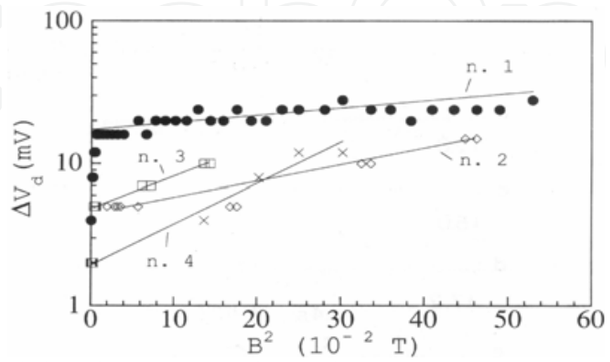

Fig. 26. Semilog plot of depolarization voltage decrease versus B^2; n corresponds to several studied neurons (Azanza and del Moral, 1996.

a ΔT small interval, at $T_{f1} \approx 30^{o}C$ and $T_{f2} \approx 37^{o}C$, corresponding to phase transitions within the membrane liquid crystal. After the second transition *f* decreases with T increase, now in agreement with (8), although *f* temperature behaviour requires a deeper investigation, and PP liquid crystal viscosity energy dissipation, $\varepsilon_v = -\eta_r(T)\theta(t)$ introduction in the SD -CE model (η_r is the membrane viscosity coefficient).

3.3 Bioelectric impulse shape and frequency spectrum.

Comparison with experiments in single neurons: we will now compare our HHM model of impulse shape (§ 1.2) with the electrophysiological experiments performed on *Helix aspersa* single unit neurons, a good bench for present studies as we have already noticed. Thus in Fig.27 we present the spontaneous ($B_{eff} = 0$) R+H voltage time time variation for two mapped neurons, fitted by the approximate solution eq. (4), the agreement being reasonable, but where we do not reproduced the sigmoidal variation at the ends, due to the series cut-off in eq. (3). The more "accurate" frequency used "sigmoidal" fit by $\left(1 - e^{-t/\tau_K}\right)^4$ is also shown, but its basis is purely phenomenological. We took $E_K = -75\,mV$, $E_{Na} = +50\,mV$ (this e.m.f. rectified by the delayed K^+ channels), $g_K = 1.6 \times 10^{-7}\,m^{-2}\,\Omega^{-2}$ and $C_m = 4 \times 10^{-2}\,Fm^{-2}$, and from the fits we obtained the n_0 and τ_K values quoted in Table 1. Clearly we can not identify parameters n_0 with the number of K-protein channels (KP), with a density of ≈ 7 KP/ μm^2, which for a neurone of 100 μm diameter yields $\approx$ 2x10^4 KP. In Fig.28 we show the frequency spectrum of a bioelectric impulse of neurone V19, together with the fitted theoretical one by eq. (5), using the parameter values of Table 1, the agreement being excellent, the same happening for other neurons (not shown). Under applied AC MF we have observed that the shape of the impulse becomes *unmodified*, which means that the solution of full integral eq. (3) with I_{Ca} inclusion is not needed. Integral eqs. (3) and (6) can be easily transformed into second order linear differential equations of well known solutions, not given here. In Fig. 28 is shown the Fourier frequency spectrum of R+H neuron impulse tram, fitted by a *Lorentzian* fuction as our model predicts (see § 3.4 below).

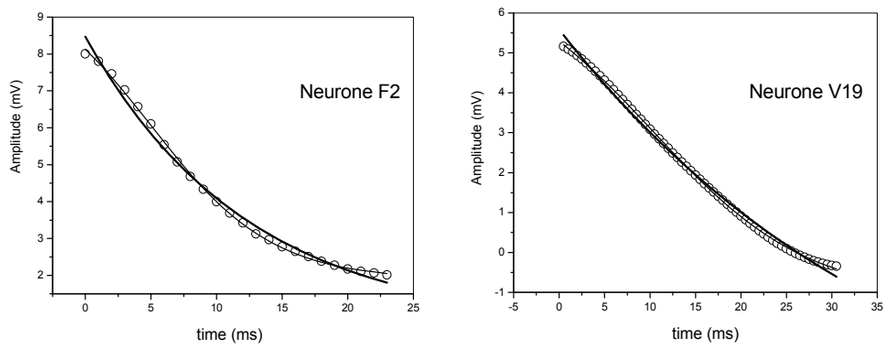

Fig. 27. Experimental (o) and model (thick line) R+H voltage time variations for neurons F2 and V19; thin line, phenomenological sigmoidal variation.

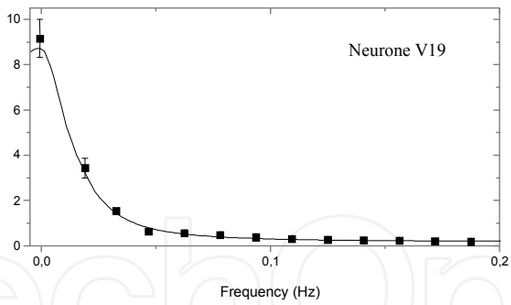

Fig. 28. Frequency Fourier spectrum of R+H impulse tram. Experiment (■) and Lorentzian, $L(f)$, model fit $\mathcal{L}(f)$ (full line).

Neurone	n_0	$\tau_K\,(ms)$	$\left(m_0^3 h_0\right)^{1/4}$	$\tau_{eff}\,(ms)$
F1	200	33.0	51	92.7
F2	188	49.4	45	149.9
V3	202	45.0	49	109.6
V14	272	12.4	58	57.0
V19	155	156.7	41	222.8

Table 1. Initial values of n, m, and h HH functions and K^+,τ_K, and Na^+,τ_{eff}, relaxation times.

Similarly in Figs. 29 we show the D voltages for the same neurons impulses, fitted by eq. (6), using the above parameter values and $g_{Na} = 1.9 \times 10^{-7}\,m^{-2}\,\Omega^{-2}$, from the fits obtaining the values of $\left(m_0^3 h_0\right)^{1/4}$ and τ_{eff} also quoted in Table 1. Values of $\left(m_0^3 h_0\right)^{1/4}$ are larger than n_0 ones, and same above consideration apply to them. Also Na^+ relaxation times, τ_{eff} are larger than τ_K, although in the impulse times $t_S < t_b$ (Fig.27) because $V_{Na}(t)$ is interrupted at the smaller (abs.value) E_{Na} than E_K for $V_K(t)$. In Fig.30 is again shown the frequency spectrum of $V_{Na}(t)$ for neurone V-19, and the fit by the corresponding *Lorentzian*. D voltage is unmodified by applied AC MF and again solving of R+D equation under MF with I_{Ca} term is not needed.

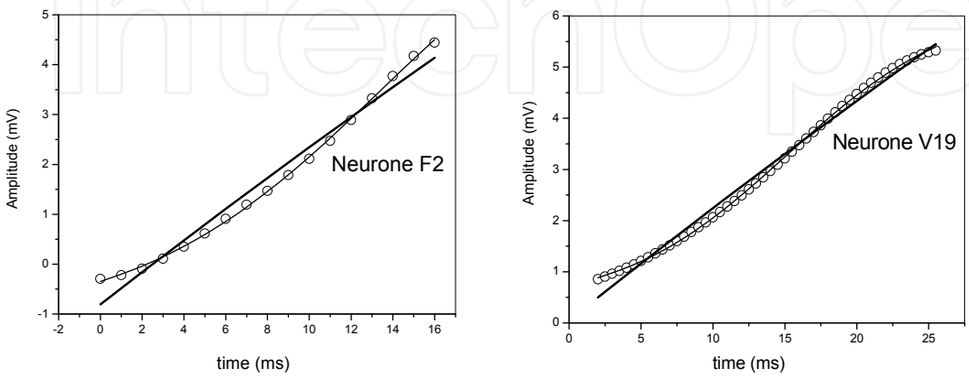

Fig. 29. Ibidem Fig. 27 for the depolarisation (D) process; lines: thick, model fit; thin, phenomenological sigmoid.

Overall our HHM model explains well the spontaneous time dependence of the bioelectric impulse and its frequency spectrum. Demonstration that AC MF produced voltage, V_{Ca} variation is negligible is a mathematical problem of HHM differential equation resolution

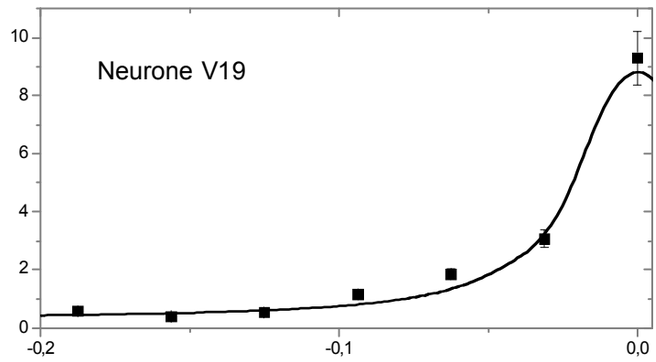

Fig. 30. Frequency spectrum (■) for impulse depolarization of neurone V-19. Line is the Lorentzian fit, $\mathcal{L}$(f).

as mentioned before. The main predicted effect of $I_{Ca}(B_{eff}, t)$ is upon the neurone bioelectric *frequency*, as we have previously shown that it occurs experimentally. Therefore we should say that the MF (either static, AC of ELF and ELF modulated MW) effect is quite *subtle* upon neuron bioelectric activity.

3.4 Magnetic field frequency dependence of biolectric activity: frequency window effect.-

The experiments initiated in 1975 by Adey and co. (Bawin et al., 1978) about the effects of ELF MF upon neural tissue are a breakthrough in the understanding of how AC ELF MF interacts with this tissue, apart from its *negligible* Joule heating. They prepared newborn chicken brain slices and embedded them in a physiological HCO_3^- water solution doped with radioactive $^{45}Ca^{2+}$ as marker. The tissue was then irradiated with a radiofrequency (RF) field of 147 MHz, *amplitude modulated* by an ELF MF (of amplitude 25 - 30 nT) in the interval 0.5 - 35 Hz, observing an increase of $^{45}Ca^{2+}$ efflux from the tissue. The experiments demonstrated two things: i) the RF (147 MHz) electromagnetic field (EMF) does *not* produce a measurable efflux increase; ii) a calcium efflux increase was observed for the tissue irradiated with the modulated wave, but only within an interval of about 5-25 Hz, so called *frequency window* effect (FWE) (see Fig.31). We have also found a FWE in *Helix aspersa* brain, irradiated with microwaves of 9.6 GHz amplitude modulated between 2-100 Hz, as already

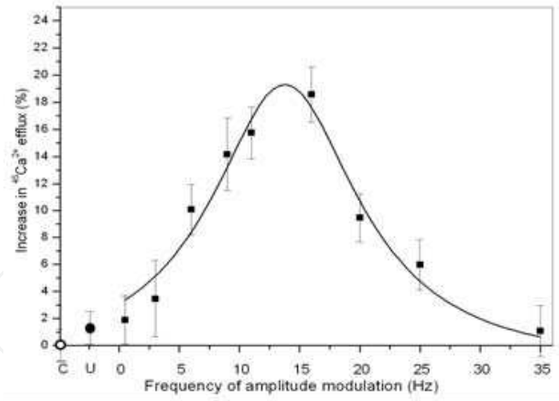

Fig. 31. The points (•) are the experimental $^{45}Ca^{2+}$ efflux increase from chicken brain under application of 147 MHz EMF carrier (intensity 0.8 mW/cm²), amplitude modulated by a MF of frequency, f_M between 0.5-35 Hz and $B_0 \cong 30$ nT (Bawin et al. 1978b). The curve is the theoretical Lorentzian, fitted according to the model eq. (9) (symbols C (O) and U (•) respectively correspond to control and unmodulated EM wave experiments.

briefly described in § 2.3.1.2. Since Ca^{2+} electrochemical gradient, E_{Ca} displaces these ions to the cell interior, the observed efflux was interpreted as Ca^{2+} liberation from the external membrane surface. FWE was afterwards found in many other kinds of cells and experimental conditions, in particular for the bioelectric *frequency*, *f* dependence with the applied ELF MF frequency, f_M in *Helix aspersa* single neurons (Pérez-Bruzón et al., 2004). Our new observation is that the calcium efflux closely follows a *Lorentzian* curve, written now in the normalized form,

$$\varphi(\omega_M) = \varphi(\omega_0)(\Delta\omega/2)^2 / \left[(\omega_M - \omega_0)^2 + (\Delta\omega/2)^2\right] \quad , \tag{9}$$

where ω_0 is the frequency at the maximum efflux $\phi(\omega_0)$. Effectively, in Fig.31 the continuous line is the fit by (9) to the experimental calcium efflux (■ points), and where $f_0 = \omega_0/2\pi \cong 14$ Hz and $\Delta f = \Delta\omega/2\pi = 14.8$ Hz.

The quantitative explanation of such a FWE, although profusely mentioned and discussed since then (Azanza and del Moral, 1994), remained unknown. Although those workers considered that the electric field of the ELF EMF was the responsible for the effect, it seems now clear that it is the magnetic field the responsible one (Pérez-Bruzón et al., 2004). This conclusion also stems from our experiments performed upon single neurons of *Helix aspersa*, submitted to an AC MF, of amplitude $B_0 = 0.1\mu$T-1 mT in the range of 0.1- 100 Hz, as above mentioned.

The *Lorentzian* frequency, f_M dependence either of the calcium efflux to the extra-cellular fluid from chicken neurons, $\phi(\omega_M)$ or the bioelectric frequency dependence $f(f_M)$ in *Helix aspersa* neurons suggest a common origin for the time dependence of the mechanism involved in the Ca^{2+} ions detaching from their binding sites and their final sequestration or capture. This dependence merely is that the amount of Ca^{2+} ions either freed to the external or to the cytosol sides from the membrane *must* vary in the form

$$N(t) = N(0)\exp(-t/\tau_{Ca}) \ , \tag{10}$$

for an applied ELF MF starting at t = 0. This is so *because the Fourier transform of a Lorentzian function is an exponentially time decaying function* (i.e. a relaxation mechanism), with relaxation time $\tau_{Ca} = 2/\Delta f$, as we have shown in §§ 1.3 (theory) and 2.3.1.2 (experiment). This is our main point in favour of a *resonance* effect for the FWE. The time τ_{Ca} is the one required for performing the process of Ca^{2+} liberation from its membrane binders, mainly Ca^{+} diffusion within the external or cytosol fluids and final Ca^{2+} sequestration either by a protein channel (or by other cytosolic structures) or incoming to the radioactivity counter for the externally freed $^{45}Ca^{2+}$ ions. In their diffusion the Ca^{2+} ions traverse an Einstein RMS distance $\sqrt{\langle \ell^2 \rangle} \cong \sqrt{D\,\tau_{Ca}}$, the one for a random walk, where *D* is the diffusion coefficient of the ion in the fluid (see e.g. Nelson, 2004). Therefore we come up with $N(t)$ obeying a dynamic equation of relaxation $dN/dt = -N/\tau_{Ca}$, as we would expect for a *two states* system (freed Ca^{2+} and bonded Ca^{2+} to its sites) in stationary equilibrium, with Ca^{2+} decay between the two states. For the Ca^{2+} ions freed to the extra-cellular fluid they will end up fully thermalized and dissolved in it, increasing its concentration ($^{45}Ca^{2+}$ efflux in Adey & Bawin's experiment). For the Ca^{2+}ions liberated to cytosol, they will diffuse and finally will have a certain probability of being captured by a K^{+}-protein channel through the calmodulin (CM) attractive electric field, $\mathbf{E}_{pK}$ (see Fig.23, only acting close to CM due to the $\mathbf{E}_{pk}$ shielding beyond the Debye length, λ_D. The diffusion Ca^{2+} current density has the form

$$J_{Ca^{2+}}(t) = \left(N_{Ca^{2+}}(0) f(B_{rms}) q_{Ca^{2+}}\right) \exp\left(-t/\tau_{Ca^{2+}}\right) \tag{11}$$

where $N_{Ca^{2+}}(0)$ is the Ca^{2+} extra-concentration liberated in a supposedly Gaussian "burst", which was previously *calculated* and yields ≈ 10 times the at rest Ca^{2+} concentration.
We can quantitatively express the above considerations by Fourier transforming the observed *Lorentzian* function *L* (ω_M), which represents either the efflux $\phi(\omega_M)$ or the bioelectric frequency $\omega(\omega_M)$ dependences, around the neurone spontaneous frequency, ω_0, (or around the frequency for the maximum in the Fourier spectrum of the firing spikes wave) i.e.

$$N(t) = \int_{-\infty}^{+\infty} L(\omega_M)\ \omega\left(B_{eff} = 0\right) \exp\left(-\alpha B_{ef}^2\right) \exp\left(-i\left(\omega_M - \omega_0\right) t\right) d\omega_M = \tag{12}$$

$$\omega(B_{eff} = 0)\exp\left(-\alpha B_{eff}^2\right) \int_{-\infty}^{+\infty} \left(2(\Delta\omega/2)/\left((\omega_M - \omega_0)^2 + (\Delta\omega/2)^2\right)\right) \exp(-i(\omega_M - \omega_0)t)\, d\omega_M = \omega(B_{eff} = 0)\exp\left(-\alpha B_{eff}^2\right)\exp(-t/\tau_{Ca})$$

If we now call $N(0) = \omega(B_{eff} = 0)\exp(-\alpha B_{eff}^2)$ to the initially (at t = 0) detached Ca^{2+} ion number within a Gaussian burst, we end up with the Ca^{2+} relaxation (10) (note, in (12) $\omega(B_{eff} = 0)$ is dimensionless). Since τ_{Ca} is related to $\Delta\omega/2$, which is experimentally accessible from the $\boldsymbol{L}(\omega_M)$ spectra, we can determine that time from experiment.

The central frequency ω_0 in (12) is assumed to be the spontaneous average bioelectric frequency, so that we obtain a *resonance* or maximum of calcium efflux when $\omega_M = \omega_0$. This resonance mechanism should not be confused with the unspecific stochastic resonance model one. This model is based also on a two-states system, but assuming a critical noise

which is modulated by the AC driving agent and reaches a threshold value (see e.g. Wellens et al., 2004). A difficulty with this model is that the *physical* mechanism involved in the weak AC agent interaction with the system is neither specified nor quantified. Therefore it becomes of questionable application to the distribution of spontaneous bioelectric frequencies, $D(\omega_0)$ (Fourier spectrum) for the biological system (membrane), also *Lorentzian* (setting $\omega_M = 0$ in (9) and (12)). In fact, and beyond the spontaneous impulse Fourier transform, such a distribution has been directly inferred from our experiments with *Helix aspersa* brain neurons, in the form of repetitive narrow bursts of higher frequency (Fig.32), localized in time when f_M is increased, and superposed to the main $f(f_M)$ *Lorentzian* decrease below f_0 (Pérez-Bruzón, 2006).

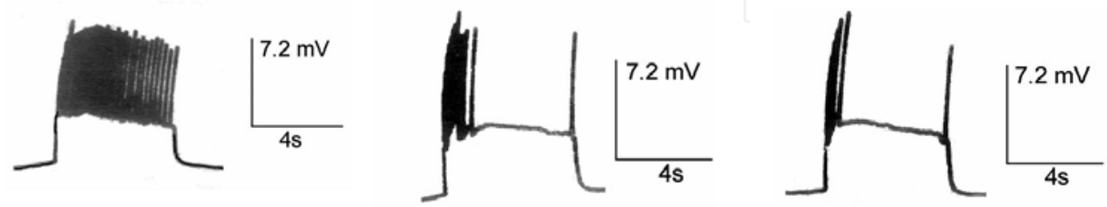

Fig. 32. Neuron D-5 spontaneous bursts of variable f, superposed to the main spike firing train.

In Fig.31 we effectively showed the excellent fit by (9) of the calcium efflux increase vs. f_M, and which means that our SD-CE and Ca^{2+} kinetics model gives a physical and *quantitative* explanation to the Adey & Bawin's FWE observation (Bawin et al., 1978). According to our assumption chicken cerebral neurons average bioelectric frequency should be $f_0 \cong 14$ impulses/s, to some extent comparable with the mollusc neurons with $f_0 \approx 0.1\text{-}8.0$ impulses/s. Similarly in Fig.33 we present the bioelectric frequency f vs. f_M variation for

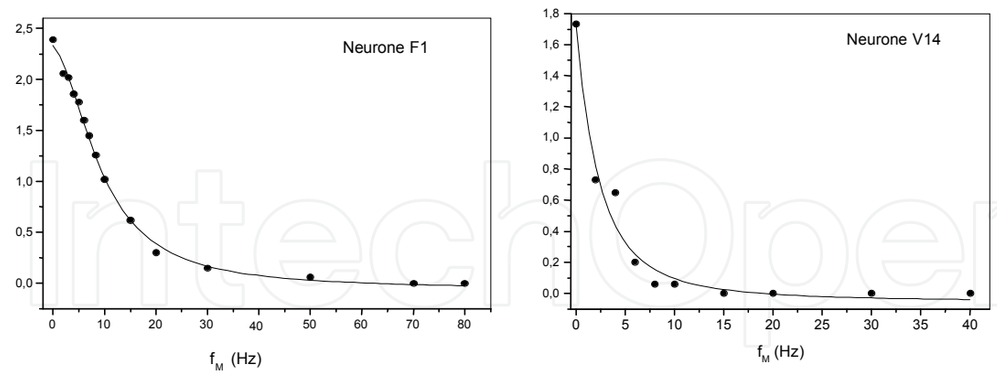

Fig. 33. Variation of bioelectric frequency, f with MF frequency, f_M. Experiment (•); lines are Lorentzian fits $L(f_M)$, with f_0=2.5, 2.0 Hz and $\Delta f/2$= 9.9, 2.7 Hz for neurons F1 and V14 respectively.

Helix aspersa brain mapped neurons F1 and V14, under AC MF of B_0=1 mT. The fit of $f(f_M)$ by $L(\omega_M)$ is also rather good. Therefore in our ELF amplitude modulated MW experiments ω_0 is the frequency corresponding to the maximum of the impulse train Fourier spectrum

(see Figs. 15b and 18b). Then the modulated MW experiments have the ability of *picking up the impulse voltage structure*, whereas AC-MF ELF experiments apparently only pick up the firing repetition frequency, f , which just decreases with increasing, f_M, although also with Lorentzian shape The reason for those different behaviours is currently unknown.

Now, as above mentioned, the bioelectric activity is commanded by the AC MF Ca^{2+} ions internally detached towards the cytosol, which join the K^+-protein channels and open them, giving rise to the bioelectric impulse of K^+ ions sorting out. Therefore this mechanism should be also operative in the chicken brain bioelectric activity, and therefore both experiments reveal the Ca^{2+} simultaneous detaching from *both surfaces* of the membrane. Bioelectric phenomena where both membrane sides are involved are known to be important in biological systems because they couple external membrane interactions with cytoplasm, our case through Ca^{2+} Coulomb explosion. Besides the determined Ca^{2+} relaxation times, τ_{Ca} are 135 ms (chicken brain) and between 93-365 ms for the studied neurons of *Helix aspersa.* An *ab-initio* calculation of the Ca^{2+} relaxation time, τ_{Ca} is difficult, if we consider the mentioned above kinetics involved. In fact a first principles calculation of the K^+ and Na^+ relaxation times in HH equations is still an open problem, relaxation times left as adjustable parameters as we assumed in § 2.3.1.2. However for τ_{Ca} if we estimate the mean diffusion length of Ca^{2+} in water, taking $D \approx 10^{-9}\ m^2 s^{-1}$, the typical diffusion coefficient for small molecules in water (see e.g. Nelson, 2004), we obtain $\sqrt{\langle \ell^2 \rangle} \approx 30-60\ \mu m$, which are reasonable values for the studied neurons of average diameter $d \approx 100\ \mu m$ (Kerkut et al., 1975; Azanza et al., 2002). This agreement is a good crosschecking of our model.

A final check of the SD-CE model suitability is the obtaining of the cluster PP numbers, N_c in *Helix aspersa* neurons. This was done in § 3.2 from our applied SMF experiments (Fig. 34). This can be done also by determining the parameter α from the slopes of the above linearized $f(B_0)$ mentioned plots (§ 3.2) from time synchronized neurone pairs under f_M = 50 Hz MF field (Azanza et al., 2002; Azanza et al., 2005) (also from the SMF experiments of Fig. 24). In Fig. 34 are shown such a plots for the pair V13-V23 of the visceral ganglion. Taking $\chi_\perp \cong -0.56 \times 10^{-7}$, determined in erythrocyte membranes by combined SQUID

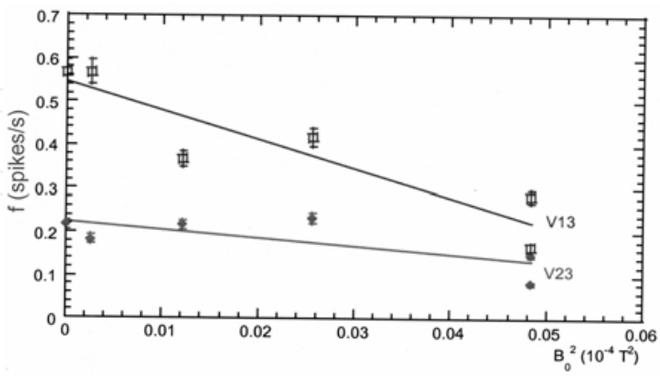

Fig. 34.- Plots of the bioelectric frequency, f vs. B_{eff}^2 (f_M = 50 Hz) for *Helix aspersa* neurone pair V23-V13 (mapped by Kerkut et al., 1975), showing *synchronization* under MF. From the line slopes is determined the α parameter. Notice the f coincidence for $B_0 \cong 2$ mT.

magnetometry ($\Delta\chi$) and electrophysiological experiments as mentioned before (del Moral and Azanza 1992; Azanza et al., 1993), $V \approx 5\times10^{-28}\,m^3$, $T \cong 293K$ and α values, obtained from the slopes, we respectively obtain $N_c \approx 4$ and 1 $x10^{12}$ PP in a membrane cluster. Considering that the numbers of PP in such a membranes, of average diameters 120 and 103 μm respectively, are $N_{pp} \approx 2$ and 1.5 $x10^{11}$ (Azanza et al., 2002; Azanza et al., 2005), that numbers throw about $c = N_c/N_{pp} \approx 42$ and 16 correlated neurons respectively, firing in *synchronized* way with the probe ones, i.e. forming "giant" PP clusters of linear extension $\approx 300\,\mu m$ (the visceral ganglion has a diameter of about 600 μm and *Helix* brain has $\approx 2\times10^4$ neurons) (Kerkut et al., 1975). Therefore neurones *form correlated small networks* under ELF weak MF, a noticeable effect. The synchronizing mechanism beyond a single neuron is mediated by the glia tissue connecting proteins, which connect in between the phospholipids membranes of two adjacent neurons via a "domino effect" of rotating PP. Observation of the existence of such connections in *Helix* brain ganglia using immunocytochemistry techniques has been actually realized (Azanza et al., 2007).

3.5 The demodulating neurone membrane.

A main issue is indeed to provide for an explanation of why the neurone only senses the low frequencies, f_M when an *amplitude modulated* magnetic field, B(t) of MW high frequency (carrier, f_c) is applied, in the form,

$$B(t) = B_c[1 + m\cos\omega_m t]\cos\omega_c t \equiv B_c[1 + G(t)]\cos\omega_c t \tag{13}$$

were $m=B_m/B_c$ is the modulation ratio, $G(t) = m\cos\omega_m t$, $B^{(m)} = B_0^{(m)}\cos\omega_m t$ is the ELF modulating MF and B_c the MW carrier MF amplitude. Our proposed model is based again on the Ca^{2+} detaching magnetic torque, quadratic (*non-linear*) in B, and Ca^{2+} diffusion within the cytosol, mainly the latter. As it is well known any demodulation process, i.e. elimination of the carrier wave, passes through the existence of some non-linear characteristic of the demodulating device. Those processes operate in fact as a detection or demodulating "device", although rather unusual and peculiar, as follows.

The diamagnetic energy of a PP cluster under modulated field B(t) is given by

$$E_M = -\left(VN_{eff}^c/2\mu_0\right)B(t)^2\left[\chi_\perp + \Delta\chi\cos^2\theta(t)\right] \tag{14}$$

where N_{eff}^c is the Ca^{2+} detaching effective number of PP in a cluster, as explained in § 3.2. Therefore the magnetic torque upon a PP cluster (in fact upon the applied field induced magnetic moment) becomes $\Gamma_M = -(\partial E_M/\partial\theta) = \Gamma_0 \sin 2\theta \sin 2B(t)^2$, where $\Gamma_0 \cong V\Delta\chi N_{eff}^c/2\mu_0$ and

$$B(t)^2 = (B_{rms,c}^2)[1 + 2G(\omega_m t) + G^2(\omega_m t)](1 + \cos(2\omega_c t)) \tag{15}$$

Therefore the acting magnetic torque, Γ_M has two components: i) The carrier frequency, f_c (modulated) torque:

$$\Gamma_c = F\,(1 + 2G + G^2)\,B_{rms,c}^2\cos2\omega_c t \tag{16}$$

purporting the high frequencies $2\omega_c$, $2\omega_c \pm \omega_m$, $2\omega_c \pm 2\omega_m$, and where $\omega_m/\omega_c \approx 10^{-8}$ and $F \equiv \Gamma_0 \sin 2\theta$. ii) The modulating frequency, f_M field torque

$$\Gamma_m = F\, B^2_{rms,c}\left[1 + 2G(\omega_m t) + G^2(\omega_m t)\right] , \tag{17}$$

with ELF $\omega_m = 2\pi/f_m$. Now the angle θ(t) between the PP axis and MF **B** has a complicated motion equation to solve, mainly because of the complex time dependent Ca^{2+}-Ca^{2+} Coulomb repulsion torque $\Gamma_{rep}(\theta)$. The motion equation is

$$I_{pp}\ddot{\theta}(t) + \beta\dot{\theta}(t) + \kappa\theta = \Gamma_M(\theta) + \Gamma_{rep.}(\theta) \tag{18}$$

where I_{pp} is the PP inertia moment, β the PP rotation damping coefficient (mainly due to membrane viscosity) and κ the restoring parameter representing the Coulomb Ca^{2+}- Ca^{2+} repulsion, although the PP rotate as a cooperative cluster due to superdiamagnetism.
We will assume no PP acceleration, weak viscosity in the PP membrane and weak Coulomb repulsion (except at the short distance of the Coulomb explosion), and then we may assume that PP follows the applied field and then $\theta(t) \cong \omega_{field} t$ .Therefore the effective torque finally becomes of the form

$$\Gamma_M = \{\Gamma_c(t) + 4\Gamma_0 B^{(m)}_{rms} B^{(c)}_{rms} \cos\omega_m t + \Gamma_0 B^{(m)\,2}_{rms} \cos^2\omega_m t\} \sin 2\theta(t). \tag{19}$$

Now the main model assumption is that when period of the carrier torque, $T_c \approx 75$ps is much smaller that the Ca^{2+} relaxation (diffusion) time, τ_{Ca} (100-400 msec) towards the K^+ channel (or other cytosolic sites), the detached Ca^{2+} ion is recaptured and it is ineffective: *so carrier torque becomes rectified.* However there can be effective detaching with the modulating field, since its period, T_m and τ_{Ca} are comparable, i.e. $\tau_{Ca} \approx 100 - 350$ms against $T_m \approx 1$ s - 100 ms or $T_m/2$.
Therefore the *only effective* torque for an effect of ELF MWmodulated MF on a PP membrane is:

$$\Gamma^{eff}_M = (V\Delta\chi N^c_{eff}/\mu_0)\{\tfrac{2}{m} B^{(m)\,2}_{rms} \cos^2\omega_m t \cdot \sin\omega_m t + B^{(m)\,2}_{rms} \cos^3\omega_m t \cdot \sin\omega_m t\} . \tag{20}$$

A schematic picture of the two magnetic torque components in (20) is shown in Fig.35, where only in the non-hatched time intervals in each T_m period, Ca^{2+} detaching occurs because of the favourable PP Ca^{2+} charged heads positions (see skechted drawings). Therefore (20) expresses that the only MF being "effectively" acting upon the neuron (membrane) is the ELF modulating one, the magnetic torque acting upon the PP membrane plus Ca^{2+} diffusion and sequestration being both the demodulating cell membrane "device". Our current model does not include thermal effects in the demodulation process since Peierls energy barrier between the two Ca^{2+} states has been omitted on a first approximation. Summarizing we propose that the combined action of the *non-linea*r in field, **B** magnetic torque upon the PPs, which liberate Ca^{2+} from the inner membrane surface plus the *slow diffusion* of Ca^{2+} towards the K^+ channels in order to open them, constitute the *demodulation mechanisms* in membranes in order to the membrane *sensing only the ELF modulating signal*.

Fig. 35. The two components of the rectified effective torque acting upon a phospholipid cluster. Ca^{2+} detaching only occurs for the $T_m=1/f_m$ period times interval shown. For the grey marked times detaching does not occur. Also showns in the Ca^{2+} diffusion current, given by [11].

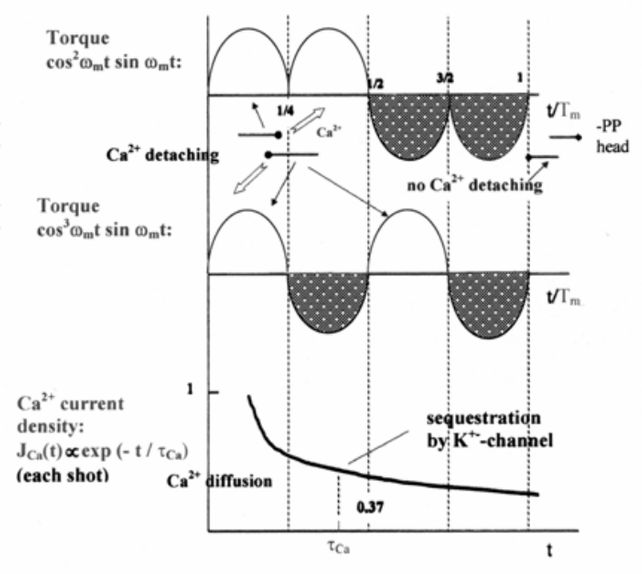

Fig. 35. The two components of the rectified effective torque acting upon a phospholipid cluster. Ca^{2+} detaching only occurs for the $T_m=1/f_m$ period time intervals shown in white. For the grey marked times detaching does not occur. Also shown is the Ca^{2+} diffusion current, given by (11).

4. Conclusions

In this chapter we have shown that the main effect of low strength MF (static, alternating of ELF and ELF MF modulated MW) upon neural tissue is the modification of the neuron bioelectric activity *frequency*, either reducing or increasing it depending on the neuron nature. The general underlying mechanism is the *Ca^{2+} ion liberation from the cytosolic membrane through a mechanism which involves the phospholipid (PP) field induced diamagnetism, the cooperative PP action superdiamagnetism, the Ca^{2+} ion Coulomb explosion from their membrane stores, either increasing the cytosol charge (bioelectric frequency excitation) or reducing the firing frequency (inhibition process) through the Ca^{2+} opening of K^+ channels*. This has been proved by comparing our electrophysiological experiments with our purposely made biophysical model, which explains in a fully quantitative way the performed experiments. A model is also presented which shows how *the neuron membrane acts as a demodulating system* for the ELF amplitude modulated applied MW and that also underlines the superdiamagnetic effect, the Ca^{2+} liberation and the *non-linear* dependence with the MF strength, B of the upon PP's exerted magnetic torque. Demodulation of ELF modulated MW in neurons becomes in this way a rather subtle mechanism, manifested in the form of the observed *frequency resonances* (no of "spring kind") of membrane with the applied ELF MF modulating the MW carrier. Neuron membranes more than acting as amplifying structures for the

electromagnetic wave interaction behaves as cooperative diamagnetic structures in their interaction with either static or dynamic *low frequency* magnetic fields.

ACKNOWLEDGEMENTS

We are grateful to Professor R. Gómez and co. of University of Granada for the MW dosimetry simulations. We gratefully acknowledge financial support from the Spanish Ministry of Defence under Project ERG 101.103, from the "Fundación Humanismo y Ciencia" (Madrid) and from "Diputación General de Aragón" under Project B43.

5. References

Adey, W.R. (1986). The sequence and energetics of cell membrane transductive coupling to intracellular enzyme systems. *Bioelectrochem.Bioenergetics*, 15, 447-456.

Adey, W.R. (1988a). Electromagnetic fields, cell membrane amplification and cancer promotion. In: *Non-ionizing Electromagnetic Radiations and Ultrasound*, pp. 80-110. Ed.NCRP: Bethesda.

Adey, W.R. (1988b). Cell membranes: The electromagnetic environment and cancer promotion. *Neurochem. Res*. 13, 671-677.

Alberts, B.; Bray, D.; Lewis, J.; Raff, M.; Roberts, K. & Watson, J.D. (1989). In: *Molecular Biology of the Cell*. Garland: New York.

Axelrod, J.; Burch, R.M. & Jelsema, C.L. (1988). Receptor-mediated activation of phospholipase A2 via GTP-binding proteins: Arachidonic and its metabolites as second messengers. *Trends Neurosci*. 11, 117-123.

Azanza, M.J. & del Moral, A. (1988). Effects of static magnetic fields on isolated neurons. *J. de Phys.* (París). 12: C8-2059-2060.

Azanza, M.J. (1989). Steady magnetic fields mimic the effect of caffeine on neurons. *Brain Res*. 489: 195-198.

Azanza, M. J. (1990). Characterization of neuronal membrane K^+ and Ca^{2+} channels operated under steady magnetic fields exposure. *J.Magn.Magn.Mat*. 83: 527-529.

Azanza, M.J., Blott, B.H. del Moral, A., and Peg, M.T. (1993). Measurement of the red blood cell membrane magnetic susceptibility. *Bioelectrochem. Bionergetics.* 30: 45-53.

Azanza, M.J. & del Moral, A. (1994). Cell membrane biochemistry and neurobiological approach to biomagnetism. *Prog.Neurobiol. 44*: 517-601. Review.

Azanza, M.J. & del Moral, A. (1995). Neuron firing frequency dependence on the static magnetic field intensity. *J. Magn.Magn.Mat.* 140-144, 1464-1465.

Azanza, M.J. & del Moral, A. (1996). Isolated neuron amplitude spike decrease under static magnetic fields. *J. Magn. Magn. Mat*. 157-158: 593-594.

Azanza, M.J. & del Moral, A. (1998). ELF-magnetic field induced effects on the bioelectric activity of single neurone cells. *J. Magn. Magn. Mat.* 177-181: 1451-1452.

Azanza, M.J.; Calvo, A.C. & del Moral, A. (2001). 50 Hz Sinusoidal Magnetic fields induced effects on the bioelectric activity of single unit neurone cells. *J.Magn.Magn.Mat. 226*-230: 2101-2103.

Azanza, M.J.; Calvo, A.C. & del Moral, A. (2002). Evidence of synchronization of neurons activity of molluscan brain ganglia induced by alternating 50 Hz applied magnetic field. *Electro-Magnetobiology*. 21: 221-232.

Azanza, M.J.; Pérez-Bruzón, R.N.; Calvo, A.C. & del Moral A. (2005). Elemental neuron network dynamics under applied sinusoidal magnetic fields, Proceedings of BioEM 2005, pp. 312-314, June 19-24, Dublín, Ireland.

Azanza, M.J.; Pes, N.; Pérez-Bruzón, R.N.; Aisa, J.; Raso, M.; Junquera, C.; Lahoz, M.; Maestú, C.; Martinez-Ciriano, C.; Pérez Castejón, C.; Vera Gil, A. & del Moral, A. (2007a). Localization of connexins and glia cells of the Helix aspersa suboesophageal brain ganglia by immunocitochemistry. *Histol.Histopathol*. 22: 497-504.

Azanza, M. J.; Pérez-Bruzón, R .N. & del Moral, A. (2007b). Frequency resonance effect of under low-frequency weak magnetic fields. *J. Magn. Magn. Mat*. 310**:** 2865-2867.

Azanza, M.J.; Pérez Castejón, C.; Pes, N.; Pérez-Bruzón, R.N.; Aisa, J.; Junquera, C.; Maestú ,C.; Lahoz, M.; Martinez Ciriano, C.; Vera Gil, A. & del Moral, A. (2008). Characterization by immunocytochemistry of ionic channels in *Helix aspersa* suboesophageal brain ganglia. *Histol. Histopathol*. 23 397-406.

Azanza, M.J.; Calvo, A.C.; Pérez-Bruzón RN, Maestú, C. & del Moral, A. (2009). Neuron network dynamics under applied low frequency magnetic fields. Submitted.

Babu, Y.S.; Sack, J.S.; Greenough, T.J.; Bugg, C.E.; Means, A.R. & Cook, W.J. (1985). Three-dimensional structure of calmodulin. *Nature*. 315: 37-40.

Bawin, S.M.; Sheppard, A. & Adey, W.R. (1978). Possible mechanism of weak electromagnetic field coupling in brain tissue. *Bioeletrochem. Bioenergetics*. 5: 67-76.

Berridge, M.J. & Irvine, R.F. (1984). Inositol triphosphate, a novel second messenger in cellular signal transduction. *Nature* 312, 315-321.

Bleany, B.I. & Bleany, B. (1965). Electricity and Magnetism. Oxford University Press: Oxford

Calvo, A.C. & Azanza, M.J. (1999). Electrophysiologic responses of snail under applied 50 Hz alternating magnetic fields. *Electro- Magnetobiology*. 18: 305-312.

Calvo, A.C. (2006). Doctoral Thesis. University of Zaragoza, Spain, unpublished.

Cole, K.S. & Curtis, H.J. (1939). Electric impedance of the squid giant axon during activity. *J.Gen.Physiol*. 22, 649-670.

del Moral, A. & Azanza, M.J. (1992). Model for the effect of static magnetic field. *J. Magn. Magn. Mat*. 114: 240-242.

del Moral, A.; Azanza, M.J. & Pérez–Bruzón, R.N. (2006). Models of neurone dynamics: spontaneous and under ELF alternating magnetic fields. "4th International Workshop: Biological Effects of EMFs", ISBN 960-233-172-0, pp-594-603, Creta, 2006.

del Moral, A.; Pérez-Bruzón, R.N. & Azanza, M.J. (2008). Frequency windows in neurones under low frequency modulated microwaves. *Proc. of the 38th European Microwave Conference, Amsterdam, The Netherlands, 27-31 Oct.* Ed Horizon House Publications Ltd, pp 83-86.

Downes, C.P. (1983). Inositol phospholipids and neurotransmitter-receptor signalling mechanisms. *Trends Neurosci*. 6, 313-316.

Eberhard, D.A. & Holz, R.W. (1988). Intracellular Ca^{2+} activates phospholipase C. *Trends Neurosci*. 11, 517-521.

Hinrikus, H.; Bachmann, M.; Tomson, R. & Lass, J. (2005). *The Environmentalist* **25,** 187.

Hodgkin, A.L. & Huxley, A.F. (1952). A quantitative description of membrane current and its application to conduction and excitation in nerve. *J.Physiol*. 117, 500-544.

Irvine, R.F. (1982). How is the level of free arachidonic acid controlled in mammalian cells?. *Biochem.J*. 204, 3-16.

Kerkut, G.A.; Lambert, J.D.C.; Gayton, R.; Loker, J.E. & Walker, R.J. (1975). Mapping of nerve cells in the ganglia of *Helix aspersa* . *Comp. Biochem. Physiol*. 50A: 1-25.

Leszczynski, D.; Joenväärä, S.; Reivinen, J. & Kuokka, R. (2002). Non-thermal activation of the hsp27/p38MAPK stress pathway by mobile phone radiation in human endothelial cells: molecular mechanism for cancer and blood-brain barrier-related effects. *Differentiation* 70, 120-129.

Loeb, L.A. & Gross, R.W. (1986). Identification and purification of sheep platelet phospholipase A_2 isoforms. Activation by physiologic concentrations of calcium ions. *J. Biol.Chem*. 261, 10467-10470.

Nahorski, S.R. (1988). Inositol phosphates and neuronal calcium homeosthasis. *Trends Neurosci*. 11, 444-448.

Nelson, P. (2004). *Biological Physics, Energy, Information, Life*, Freeman, New York.

Nishizuka, Y. (1984). The role of protein kinase C in cell surface signal transduction and tumor promotion. *Nature* 308, 693-698.

Ordway, R.W. ; Singer, J. & Walsh, J.V. (1991). Direct regulation of ion channels by fatty acids. *Trends Neurosci*. 14, 96-100.

Papahadjopoulos, D. & Bangham, A.D. (1966). Biophysical properties of phospholipids. II Permeability of phosphatidylserine liquid crystals to univalent ions. *Biochem. Biophys.Acta* 126, 185-188.

Pérez Castejón, C.; Pérez-Bruzón, R.N.; Llorente, M.; Pes, N.; Lacasa, C.; Figols, T.; Lahoz, M.; Maestú, C.; Vera, A.; del Moral, A. & Azanza, M.J. (2009). Exposure to ELF-pulse modulated X-band microwaves increases *in vitro* human astrocytoma cells proliferation. *Histol.Histopathol*. *in press*.

Pérez-Bruzón, R.N.; Azanza, M.J.; Calvo, A.C. & del Moral, A. (2004). Neurone bioelectric activity under magnetic fields of variable frequency in the range of 0.1-80 Hz. *J. Magn.Magn.Mat.*272-276, 2424-2425.

Pérez-Bruzón, R.N. (2006). Doctoral Thesis. University of Zaragoza, Spain, unpublished.

Pérez-Bruzón R.N.; Pérez Castejón, C.; Llorente, M.; Pes, N.; Lacasa, C.; Figols, T.; Lahoz, M.; Maestú, C.; Vera Gil, A.; del Moral A & Azanza, M.J. **(**2009). Design, dosimetry analysis and validation of an incubator for the exposure of *in vitro* human astrocyte cells to X-band microwaves in a GTEM-cell. Submitted 2009.

Pipkin, J.L.; Hinson, W.G.; Young, J.F.; Rowland, K.L.; Shaddock, J.G.; Tolleson, W.H.; Duffy, P.H. & Casciano, D.A. (1999). Induction of stress proteins by electromagnetic fields in cultured HL-60 cells. *Bioelectromagnetics* 20, 347-357.

Rothman, J.E. & Lenard, J. (1977). Membrane asymmetry. *Science* 195, 743-753.

Singer, S.J. & Nicolson G.L.(1972). The fluid mosaic model of the structure of cell membranes. *Science* 175, 720-731.

Sutherland, E.W. (1972). Studies on the mechanism of hormone action. *Science*, 177, 401-408.

Takuma, K.; Baba, A. & T. Matsuda. (2004). Astrocyte apoptosis: implications for neuroprotection. *Prog. Neurobiol*. 72, 111-127.

Wellens, T.; Shatokhin, V. & Buchleitner, A. (2004). Stochastic resonance. *Rep. Prog. Phys*. 67: 4545.

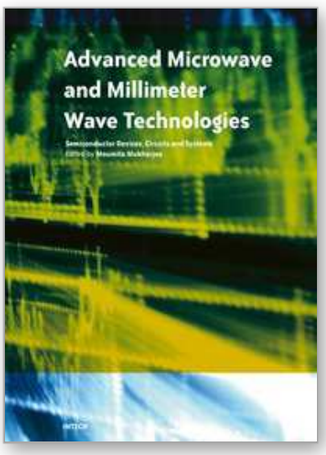

Advanced Microwave and Millimeter Wave Technologies
Semiconductor Devices Circuits and Systems
Edited by Moumita Mukherjee

ISBN 978-953-307-031-5
Hard cover, 642 pages
Publisher InTech
Published online 01, March, 2010
Published in print edition March, 2010

This book is planned to publish with an objective to provide a state-of-the-art reference book in the areas of advanced microwave, MM-Wave and THz devices, antennas and systemtechnologies for microwave communication engineers, Scientists and post-graduate students of electrical and electronics engineering, applied physicists. This reference book is a collection of 30 Chapters characterized in 3 parts: Advanced Microwave and MM-wave devices, integrated microwave and MM-wave circuits and Antennas and advanced microwave computer techniques, focusing on simulation, theories and applications. This book provides a comprehensive overview of the components and devices used in microwave and MM-Wave circuits, including microwave transmission lines, resonators, filters, ferrite devices, solid state devices, transistor oscillators and amplifiers, directional couplers, microstripeline components, microwave detectors, mixers, converters and harmonic generators, and microwave solid-state switches, phase shifters and attenuators. Several applications area also discusses here, like consumer, industrial, biomedical, and chemical applications of microwave technology. It also covers microwave instrumentation and measurement, thermodynamics, and applications in navigation and radio communication.

INTECH
open science | open minds

InTech Europe
University Campus STeP Ri
Slavka Krautzeka 83/A
51000 Rijeka, Croatia
Phone: +385 (51) 770 447
Fax: +385 (51) 686 166

InTech China
Unit 405, Office Block, Hotel Equatorial Shanghai
No.65, Yan An Road (West), Shanghai, 200040, China
中国上海市延安西路65号上海国际贵都大饭店办公楼405单元
Phone: +86-21-62489820
Fax: +86-21-62489821

IntechOpen

IntechOpen